



University of  
Massachusetts  
Amherst

## Cell-Based Sensing of Endocrine Disrupting Substances Using Fluorescent Protein-Gold Nanoparticle Complexes

Item Type	Thesis (Open Access)
Authors	Wang, Xian
DOI	<a href="https://doi.org/10.7275/5409275">10.7275/5409275</a>
Download date	2026-03-13 01:08:31
Link to Item	<a href="https://hdl.handle.net/20.500.14394/33543">https://hdl.handle.net/20.500.14394/33543</a>

**Cell-based sensing of endocrine disrupting substances using fluorescent  
protein-gold nanoparticle complexes**

A Thesis Presented

by

XIAN WANG

Submitted to the Graduate School of the  
University of Massachusetts Amherst in partial fulfillment  
of the requirements for the degree of  
MASTER OF SCIENCE

May 2014

Chemistry

**Cell-based sensing of endocrine disrupting substances using fluorescent  
protein-gold nanoparticle complexes**

A Thesis Presented

by

XIAN WANG

Approved as to style and content by:

---

**Vincent M. Rotello**, Chair

---

**Craig T. Martin**, Member

---

**Craig T. Martin**, Head  
Department of Chemistry

## ACKNOWLEDGEMENTS

In the past few years I experienced the most difficult times in my life. I would like to thank people mentioned here who had offered great support and help to me.

First, I would like to express my deep and sincere gratitude to my advisor Prof. Vincent M. Rotello, University Distinguished Professor, for his guidance and intellectual discussion. I felt lucky and honored to work in his lab even only for one year and a half. Without his help, I could still suffer from my miserable life. He gave me hope and a second chance to rebuild my career life.

I am also extremely thankful to my research committee member, Prof. Craig T. Martin for his gentle academic suggestions and personal encouragement.

I thank my present group members in Rotello's group for their friendship and collaboration. I would like to specifically thank Rui for all of his helpful advice, training, collaboration and friendship, and also Gülen for her support and collaboration during my research time. Also, my warm thanks also go to Krish, Daniel, Ying, Rubul, Moumita, Ryan, NLe, Dr. Sung Tae Kim, Dr. Chang Soo Kim, and Dr. Colleen M. Alexander for their academic suggestions.

I would like to acknowledge my friends at Amherst for their support and friendship over the years.

At last, I want to express a very heartfelt thank-you to my parents and Yuan for all their unrelenting love, patience, inspiration, motivation and constant support.

## ABSTRACT

### **Cell-based sensing of endocrine disrupting substances using fluorescent protein-gold nanoparticle complexes**

May 2014

XIAN WANG, B.S., NANJING UNIVERSITY

M.Sc., NEW MEXICO STATE UNIVERSITY

M.Sc., UNIVERSITY OF MASSACHUSETTS AMHERST

Directed by: Professor Vincent M. Rotello

Developing a sensitive and effective *in vitro* bioassay to detect endocrine disrupting chemicals (EDCs) would reduce the cost, eliminate the possibility of low dose effects, detect the non-monotonic dose responses, and identify mechanisms of actions. The “chemical nose” sensing method using supramolecular complexes composed of cationic monolayer functionalized gold nanoparticles (AuNPs) and fluorescent proteins (FPs) can successfully distinguish serum proteins, mammalian cells, tissue lysates, and chemotherapeutic drug mechanisms. EDCs regulate target cells via genomic or non-genomic pathways in terms of proliferative effect and response time. In this thesis, green fluorescent protein-gold nanoparticle (GFP-AuNP) sensors were used to detect the proliferative effect of 17 $\beta$ -estradiol (E2) and bisphenol A (BPA) on MCF7 and T47D cell lines at fM or pM dose range. Non-monotonic dose responses were also observed at different exposure times. The dose-response relationships using GFP-AuNP sensors could be correlated to the cell cycle analysis. Interestingly, tamoxifen, an estrogen antagonist, showed distinct patterns at low doses on HepG2 cells using triple channel FP-AuNP sensors, which might indicate different mechanisms of actions in this dose range.

## TABLE OF CONTENTS

	Page
ACKNOWLEDGEMENTS .....	iii
ABSTRACT .....	iv
LIST OF TABLES .....	vii
LIST OF FIGURES .....	viii
CHAPTER	
1 CELL RESPONSE SENSING AT LOW DOSES USING MULTICHANNEL FLUORESCENT PROTEIN-GOLD NANOPARTICLE SENSORS	
1.1 Introduction.....	1
1.1.1 Gold nanoparticles for biosystem sensing.....	1
1.1.2 Interaction of gold nanoparticles with proteins.....	3
1.1.3 Array-based methods for protein, mammalian cell and tissue sensing.....	5
1.1.4 LDA: an essential tool to distinguish the fingerprint patterns and classify the particular cases into tested groups.....	6
1.1.5 High throughput screening and chemotherapeutic drugs profiling using unbiased multichannel sensors.....	8
1.1.6 Toxicology and dose-response relationship.....	10
1.2 Results and Discussion.....	12
1.2.1 Fabrication of a triple-channel fluorescent protein-gold nanoparticle sensor.....	12
1.2.2 Cytotoxicity testing of drugs by viability assays.....	15
1.2.3 Unbiased sensing at varied doses using multichannel sensors.....	16
1.3 Conclusions.....	18
1.4 Experimental Methods.....	18
1.4.1 Expression and purification of fluorescent proteins.....	18
1.4.2 Fluorescence titrations and proteins sensing.....	18
1.4.3 Threshold doses, IC <sub>10S</sub> , IC <sub>30S</sub> determination.....	19
1.4.4 Cell sensing studies using multichannel sensors.....	19
1.5 References.....	20

2	CELL-BASED SENSING OF ENDOCRINE DISRUPTING CHEMICALS USING GREEN FLUORESCENT PROTEIN-GOLD NANOPARTICLE COMPLEXES	
2.1	Introduction.....	23
2.1.1	Hormones and endocrine disrupting chemicals.....	23
2.1.2	The cellular estrogen signaling pathways.....	25
2.1.3	Low dose effects and non-monotonic dose responses.....	27
2.1.4	In vitro assays for assessing endocrine disrupting chemicals.....	29
2.2	Results and Discussion .....	31
2.2.1	Cell viability tests by GFP-AuNP sensor and conventional methods.....	31
2.2.2	Endocrine disrupting chemicals sensing using GFP-AuNP sensors.....	32
2.2.3	The mechanism of cell-based GFP-AuNP sensing strategy.....	35
2.3	Conclusions.....	37
2.4	Experimental Methods.....	39
2.4.1	Comparison of measuring cell proliferation by GFP-AuNP complexes, alamar blue reagent and Hoechst 33342 stain.....	39
2.4.2	Cell-based sensing E2 and BPA using GFP-AuNP complexes and Hoechst 33342 stain.....	39
2.4.3	Fluorescent imaging using YO-PRO-1 and PI stain.....	40
2.4.4	Flow cytometric analysis of MCF7, T47D and BT549 cells at different E2 doses.....	40
2.4.5	Cell lysate studies using GFP-AuNP complexes.....	41
2.5	References.....	41
	BIBLIOGRAPHY.....	43

## LIST OF TABLES

Table		Page
1.1	Binding constant ( $K_b$ ) and binding stoichiometry ( $n$ ) between FP and AuNPs (NP1-NP4) as determined from the fluorescence titrations.....	13
1.2	Threshold doses and IC values obtained from dose-response curves fitted to the Hill equation.....	16
2.1	The cell proliferation of MCF7 and T47D induced by E2 and BPA, were measured by GFP-AuNP sensor.....	34

## LIST OF FIGURES

Figure	Page
1.1 Schematic of the AuNP-based detection system. (Ref. 6).....	1
1.2 The aggregation of oligonucleotide-functionalized AuNPs (A), in the presence of complementary target DNA, resulting in a change of solution color from red to blue (B), can be monitored by UV-Vis spectroscopy (C). (Ref. 10).....	2
1.3 Schematic representation of the molecularly imprinted polymer (MIP) sensor array that uses a dye-displacement strategy to give a unique colorimetric response pattern for each analyte. (Ref. 12).....	3
1.4 A general scheme of surface ligands on most of the common cationic AuNPs used for interaction with biological systems.....	4
1.5 The overlap of compensation plots for protein-protein and NP-protein interactions. (Ref. 14).....	4
1.6 (a) Schematic illustration of “chemical nose” sensing strategy using GFP-AuNP complexes; (b) Structures of AuNPs used for sensing; (c) Differentiation of mammalian cells by a canonical plot of discriminant analysis. (Ref. 3).....	6
1.7 (a) Schematic illustration of the sensing procedure; (b) LDA plot of the raw fluorescence data from BT549 cells under the treatment of drugs; (c) The list of chemotherapeutic drugs classified by molecular mechanisms. (Ref. 31).....	9
1.8 (a) Schematic of the FP-AuNP complex formation and structures of the cationic AuNPs (NP1-NP5). (b) The scheme of triple-channel FP-AuNP complexes and fluorescence titration curves for 100 nM FPs with four different cationic AuNPs (NP1-NP4). The changes of fluorescence intensity were measured following the addition of AuNPs at 25 <sup>0</sup> C. The solid lines represent the curve fitting using Equation 1.1.....	12
1.9 Canonical score plots for the fluorescence patterns as obtained from LDA against four protein analytes spiked in FBS at fixed concentration (2.5 nM) with 95% confidence ellipses.....	14
1.10 Dose-response curves of DOX and TAM obtained by alamar blue assay, using 7,500 cells per well after 24 hours of drug treatments.....	15
1.11 Differentiation of cell responses to DOX and TAM at three low doses (threshold doses, IC <sub>10</sub> s, and IC <sub>30</sub> s). (a) Changes in fluorescence intensities (mean of six replicates) for two cell lines treated with DOX or TAM individually (control in 1% DMSO). (b) Canonical plots of discriminant scores with 95% confidence ellipses for all data points.....	17

2.1	Structures of selective and nonselective ER ligands. Compounds shown include E2 (nonselective activators), TAM (selective ER modulator), xenoestrogen BPA, and a selective ER downregulator ICI 182,780 (ICI).....	24
2.2	Schematic model illustrating genomic and non-genomic estrogen signaling pathways. E2 activates ER $\alpha$ and ER $\beta$ , inducing dimerization and binding to the promoters of target genes. Alternatively, other classes of TFs (transcription factors) can also be modulated by activated ERs. A small population of activated ERs at the plasma membrane (mER) interact with adaptor proteins and signaling molecules such as c-Src, and regulate rapid (non-genomic) effects or gene transcription via PI3K/AKT (phosphatidylinositol 3-kinase/protein kinase B) and MAPK (mitogen-activated protein kinase) pathways. E2, or selective ER ligands (such as G-1, ICI, and TAM), can activate intracellular GPER, which stimulates cAMP production, calcium mobilization and c-Src, which activates MMPs (matrix metalloproteinases). MMPs cleave pro-HB-EGF (pro-heparin-binding-epidermal growth factor), releasing free HB-EGF that transactivates EGFR (EGF receptor), which also in turn activates PI3K/AKT and MAPK pathways. (Ref. 5).....	25
2.3	(a) Domain organization of ER $\alpha$ and ER $\beta$ . ERs consist of N-terminal domain (NTD, in red), DNA binding domain (DBD, in green), the hinge region (D domain, in blue), ligand binding domain (LBD, in yellow), and C-terminal end (in grey). (b) Binding mode of ERE to dimeric ER $\alpha$ (PDB: 1HCQ) (c) Structures of ER $\alpha$ and ER $\beta$ bound to E2 (PDB: 1A52 and 3OLS). (Ref. 9).....	26
2.4	Examples of NMDRCs. High doses (shown by dotted line) are tested to obtain the maximum tolerated dose (MTD), the lowest observed adverse effect level (LOAEL), and NOAEL. Safety factors are applied to derive the “safe” dose. However, in the actual dose-response curves, U-shaped (A) and inverted U-shaped (B) NMDRCs shown by solid lines, the adverse effects may be observed below the “safe” dose. B represents the response of EDCs. Both endogenous and exogenous effects are present. No dose in this range can be considered safe. (Ref. 8).....	28
2.5	A representative dose response curve indicating the quantitative features of hormesis. (Ref. 15).....	29
2.6	The cell proliferation tests of MCF7 cells were performed by GFP-AuNP sensor, alamar blue reagent, and Hoechst 33342 stain. The dotted plots were linearly fitted.....	31
2.7	Dose-response relationships of MCF7 (a), T47D (b) and BT549 (c) cell lines exposed to E2, BPA and ICI using GFP-AuNP sensor and Hoechst 33342 stain. Each value is the mean of three replicates.....	33
2.8	Dose-response relationships of MCF7 cells at different exposure time of E2	

	were tested by GFP-AuNP sensor.....	34
2.9	Images of MCF7 cells stained by YO-PRO-1 (green fluorescence) and PI (red fluorescence) under different conditions: PBS buffer (a), 5 mM PB (pH 7.4) (b), and BFP-AuNP sensor in 5 mM PB (pH 7.4) (c). Scale bar: 200 $\mu$ m.....	35
2.10	Representative examples of DNA histograms obtained from BD LSR II. Green, yellow and cyan areas of histograms represent G <sub>1</sub> , S and G <sub>2</sub> /M phases.....	37
2.11	(a) Comparison of cell cycle analysis on alcohol fixed cells after exposed to E2 and E2+ICI for 24 hours. 0.1% EtOH was used as control. (b) The dose-response relationships of cell lysates using GFP-AuNP sensors. The lysates were collected after the cells exposed to E2 and E2 + ICI for 24 hours.....	38

## CHAPTER 1

### CELL RESPONSE SENSING AT LOW DOSES USING MULTICHANNEL FLUORESCENT PROTEIN-GOLD NANOPARTICLE SENSORS

#### 1.1 Introduction

##### 1.1.1 Gold nanoparticles for biosystem sensing

Gold nanoparticles (AuNPs) provide promising sensing platforms for the detection and quantification of nucleic acids, proteins, cells and other biosystems, hence playing a crucial role in disease diagnosis.<sup>1,2,3</sup> Generally, there are two functional components in sensors, a recognition element providing selective binding sites and a transducer generating signals upon binding events. These two components can be linked together through covalent bonds or in the form of self-assembled supermolecular complexes. The types of signals, mainly related to the physical properties of AuNPs, can be visible color change, fluorescence signal release, and electrochemical signal enhancement (Figure 1.1).<sup>4,5</sup> The efficiency of sensors mainly relies on the recognition and transduction processes in terms of response time, signal-to-noise ratio, selectivity, and sensitivity.<sup>7</sup>

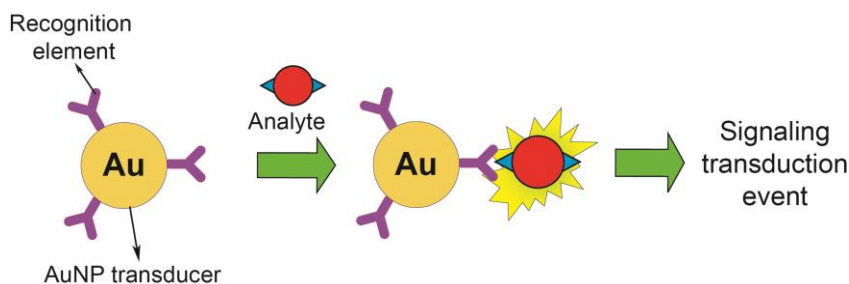


**Figure 1.1** Schematic of the AuNP-based detection system. (Ref. 6)

As an example, the aggregation of AuNPs ( $d > 3.5$  nm) inducing surface plasmon coupling can cause the visible color to change from red to blue at nanomolar concentrations.<sup>8</sup> Fabrication of AuNPs modified by thiolated DNA allows the oligonucleotide-directed AuNP aggregation for colorimetric sensing of target complementary oligonucleotides.<sup>9</sup> In this method, two ssDNA modified AuNPs were applied and both ends of target oligonucleotides were complementary to the base sequences on those two modified AuNPs. The visible color change occurred in the presence of target oligonucleotides upon DNA hybridization (Figure 1.2).

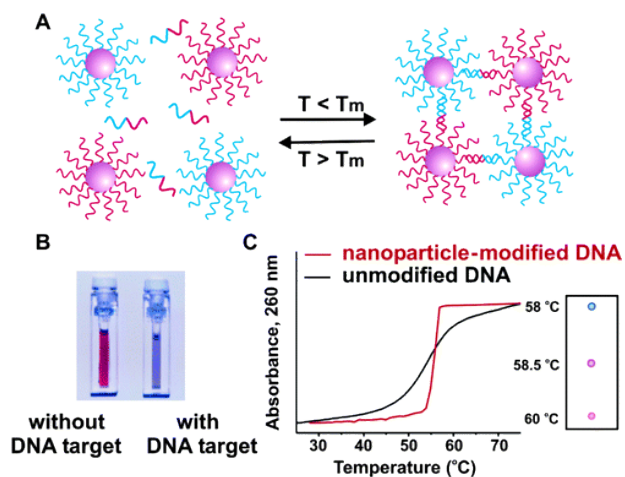


**Figure 1.2** The aggregation of oligonucleotide-functionalized AuNPs (A), in the presence of complementary target DNA, resulting in a change of solution color from red to blue (B), can be monitored by UV-Vis spectroscopy (C). (Ref. 10)

The physical properties of monolayer-protected AuNPs, such as surface functionalization, conductivity and plasmon resonance absorption, can be tuned by changing the size, shape and organic or biological ligands. As a consequence, a large variety of functionalized AuNPs of different sizes with different recognition appendages and polyvalent abilities can be achieved.<sup>11</sup>

In this thesis, we focused on the physical property of AuNPs that is the fluorescence quenching via Förster resonance energy transfer (FRET) for biosensing. The analytes in the solution are subjected to replace some or all of the fluorophores through the recognition sites of AuNPs to generate fluorescent signals. This is the general principle of indicator displacement assays (IDAs) (Figure 1.3).<sup>12</sup>

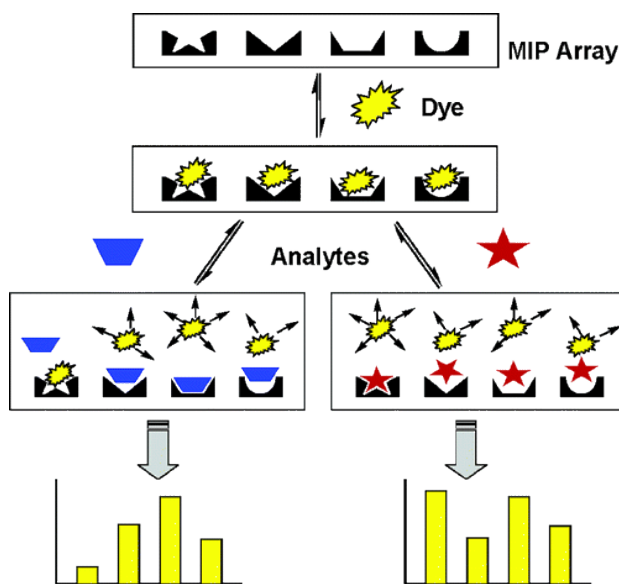


**Figure 1.3** Schematic representation of the molecularly imprinted polymer (MIP) sensor array that uses a dye-displacement strategy to give a unique colorimetric response pattern for each analyte. (Ref. 12)

### 1.1.2 Interaction of gold nanoparticles with proteins

The design and construction of monolayer-protected AuNPs is the key to the success of biosensing. We designed thiol ligands covering 2-nm-core AuNPs that are composed of three parts: a hydrophobic shell interior for the micellelike stabilization, a tetraethyleneglycol (TEG) segment for biocompatibility and the recognition elements on the exterior. (Figure 1.4) The TEG segment isolates the charged exterior headgroup layer

from the hydrophobic ligand shell interior and therefore provides the minimal requirement of limiting the protein denaturation upon binding.<sup>13</sup>

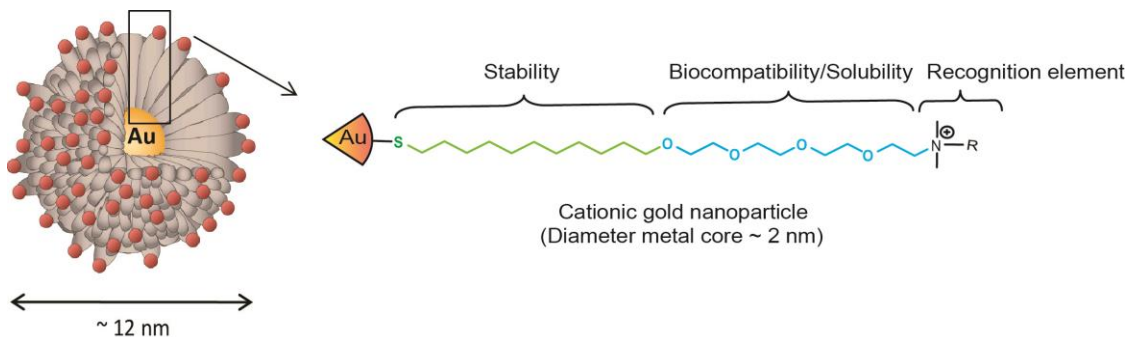


**Figure 1.4** A general scheme of surface ligands on most of the common cationic AuNPs used for interaction with biological systems.

The thermodynamic studies of amino acid-terminated AuNP-protein interactions reveal its similarity to protein-protein interactions in terms of entropy and enthalpy changes (Figure 1.5).<sup>14</sup> Appropriately modified charged AuNPs can behave as protein mimics that bind proteins reversibly. For example, AuNPs were applied to bind cytochrome c (cyt c) and disrupt the protein-protein interaction between cyt c and cyt c peroxidase.<sup>15</sup>

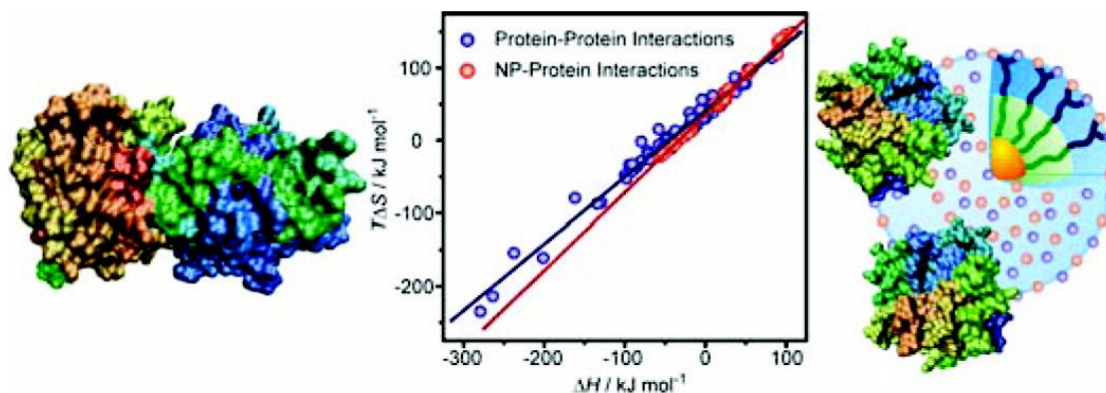


**Figure 1.5** The overlap of compensation plots for protein-protein and NP-protein interactions. (Ref. 14)

However, there are still differences between the AuNP-protein interaction and the protein-protein interaction: the monolayer-protected AuNPs offer multivalent binding sites, whereas the protein-protein interaction can be more specific like the lock and key.

Overall, tunable AuNPs provide an excellent scaffold for the recognition of target biomolecules with high affinity, which is ideal for biosensing applications.

### **1.1.3 Array-based methods for protein, mammalian cell and tissue sensing**

Based on the principle of IDAs, “chemical nose” sensor arrays, similar to series of semi-selective receptors in our olfactory systems to differentiate odors, can provide distinguishable fingerprint patterns through a composite of unbiased signals. A primary advantage of the array-based “chemical nose” sensing strategy is to rapidly identify subtle changes in sophisticated mixtures by effectively utilizing multivariate data analysis and cluster analysis. Combining a set of six AuNPs with poly(phenylene ethynylene) (PPE) polymers resulted in a distinct pattern for seven different analyte proteins.<sup>2</sup> Using linear discriminant analysis (LDA), seven different proteins at concentrations of 4 - 215 nM were identified. Remarkably, the green fluorescent protein (GFP)-AuNP complexes were able to identify five different serum proteins spiked in the undiluted human serum at a concentration of 500 nM, where the human serum albumin (HSA) concentration only changed 0.06%.<sup>16</sup> In addition, as little as 200 ng of cell or tissue lysed proteins were sufficient to distinguish disease states.<sup>17</sup> Sensing bacteria and mammalian cells covered with a complex mixture of biomolecules on their surfaces was also successfully achieved by our array-based sensing strategy (Figure 1.6).<sup>3,18,19,20</sup>

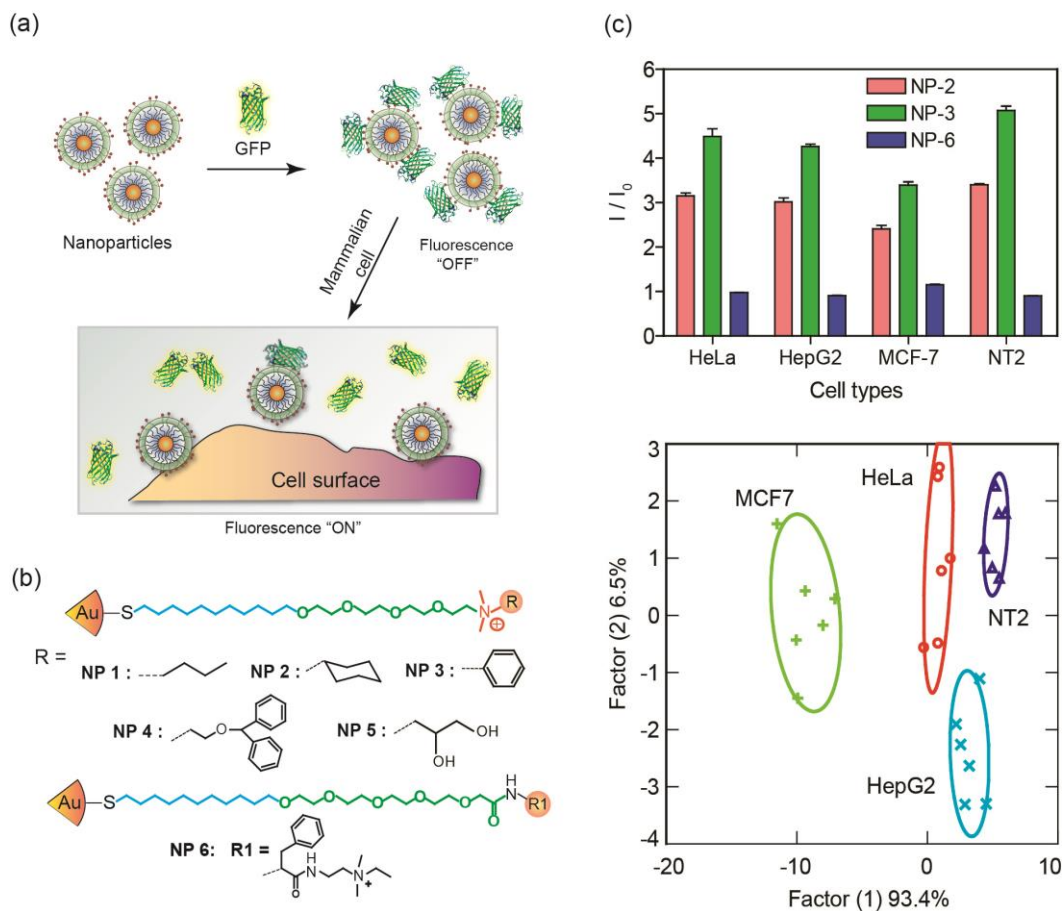


**Figure 1.6** (a) Schematic illustration of “chemical nose” sensing strategy using GFP-AuNP complexes; (b) Structures of AuNPs used for sensing; (c) Differentiation of mammalian cells by a canonical plot of discriminant analysis. (Ref. 3)

#### 1.1.4 LDA: an essential tool to distinguish the fingerprint patterns and classify the particular cases into tested groups

Linear discriminant analysis (LDA) is a multivariate data analysis method that is closely related to principal component analysis (PCA) and factor analysis. It is used to separate two or more groups of objects by performing linear combinations of independent

features or measurements (variables), such as fluorescent signals. In contrast, PCA is an unsupervised method that does not include label information of data nor take into account of any differences in groups, and factor analysis is normally used to classify variables. The form of the discriminant function is

$$D = v_1X_1 + v_2X_2 + v_3X_3 + \dots + v_iX_i + a$$

where D is the discriminant function, v is the discriminant coefficient, X is the respondent's score for that variable, a is a constant, and i is the number of variables. The number of discriminant functions is one less than the number of groups. The separation is defined as the ratio of the variance between groups to the variance within the groups.

One major aim of applying LDA is to predict to which group a particular case belongs. In general, the case is classified as belonging to the group for which it has the smallest Mahalanobis distance.<sup>21</sup> The Mahalanobis distance is a measure of distance between two points that represents the means of the group and the respective case for all variables in the multivariate space. One way to avoid the resulting inherent bias in the classification methodology is to use a jackknifed (or leaving-one-out) method.<sup>21</sup> The procedure is to determine the group classification functions when one variable is omitted and only the remaining variables are used to calculate coefficients and constants. Sometimes jackknifed classifications of each variable to each group are more reliable because they do not include that variable being classified when the classification score is calculated. Moreover, LDA can also be used to determine which variable discriminates between groups by comparing the absolute values of standardized coefficients.

### **1.1.5 High throughput screening and chemotherapeutic drugs profiling using unbiased multichannel sensors**

In drug discovery and the fields relevant to biology and chemistry, vast libraries of compounds were tested for activities against specific targets by means of high throughput screening (HTS). With manually operated workstations or fully automated robotic systems, HTS allows the testing of thousands of or millions of compounds per day. With this method one can rapidly identify active compounds, catalytic activities from purified enzymes<sup>22</sup>, antibodies<sup>23</sup>, phenotypic changes in intact cells<sup>24</sup> and genes that modulate a particular biomolecular pathway<sup>25</sup>. The HTS is viewed as the initial step of drug design and understanding the role of a particular biochemical process in biology. The secondary screens or follow-up assays are designed to use orthogonal methodology or biological readout to remove hits from initial HTS that are false positives. There are several parameters that define the format of the HTS: the nature of the signal change, the conditional stimulus, and the response time upon stimulus.<sup>26</sup> Using HTS assays in sequence can lower the possibilities of false positives in substantial secondary low throughput assays that often pertain to physiological measurements of the biological system under study.

In general, the targets of HTS involve enzymes and receptors. The major types of protein families for specific drug targets in HTS are G protein-coupled receptors<sup>27</sup> (GPCRs), kinases<sup>28</sup>, proteases<sup>22</sup>, nuclear receptors<sup>29</sup> (NRs) and ion channels<sup>30</sup>. The complexity of components and their interactions within cellular networks offering a rich source of new therapeutic targets are also assayable by HTS. For example, the specific kinase intracellular activity has been tested by phosphorylation-activated FRET sensors engineered from fluorescent protein pairs.<sup>28</sup>

Alternative to the conventional fluorescent indicators used in HTS testing specific targets or cellular pathways, FP-AuNP complexes can provide more general recognition sites but specific stimulus response patterns. One significant improvement of previous array-based chemical nose assays is to introduce multichannel FP-AuNP sensors. Its advantages are facilitating the sensing procedure, providing simultaneous fluorescent signals on the same samples and therefore eliminating the bias in the procedure of LDA.

More recently, the molecular mechanisms of apoptotic or necrotic chemotherapeutic drugs have been successfully classified by applying triple-channel FP-AuNP sensors onto BT549 cells (human breast cancer cell line) under the drug treatments (Figure 1.7).<sup>31</sup> The results imply that the phenotypic changes of cells, an adaptation in

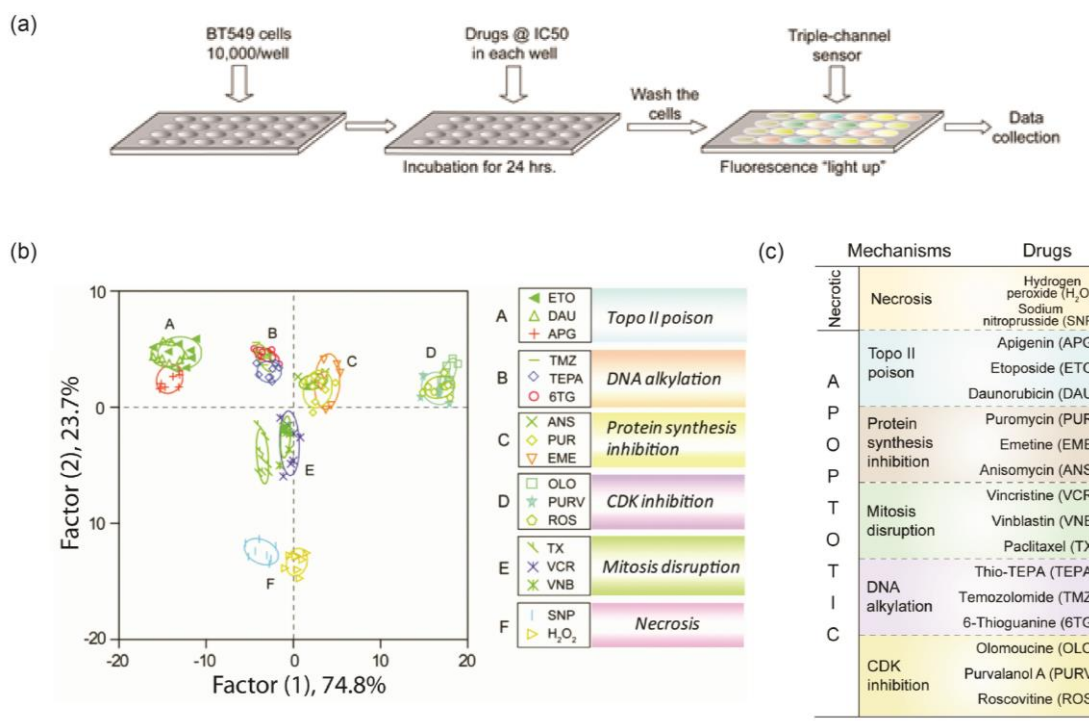


**Figure 1.7** (a) Schematic illustration of the sensing procedure; (b) LDA plot of the raw fluorescence data from BT549 cells under the treatment of drugs; (c) The list of chemotherapeutic drugs classified by molecular mechanisms. (Ref. 31)

protein expression and distribution within cellular network, can be monitored by the unbiased sensing strategy.

### **1.1.6 Toxicology and dose-response relationship**

Toxicology is the study of the adverse effects of chemicals or physical agents on human and other living organisms. The adverse effects may result in immediate death or subtle changes that are not realized until months or years later. Toxic substances or agents can affect the entire body or specific organs. There are several factors that determine adverse effects of toxic substances: intrinsic toxicity, dose, exposure conditions and host response.<sup>32</sup> Intrinsic toxicity includes the chemical and physical properties of toxic agents. The dose of a chemical or physical agent is its amount that contacts with a living organism at one time. In the words of Paracelsus (1493-1541), “All substances are poisons; there is none which is not a poison. The right dose differentiates a poison from a remedy.” Studying dose-response relationship is fundamental and essential in toxicology. In this relationship, there is almost always a dose, known as the threshold dose, below which no response occurs, and once the maximum response is reached, no more increased effects will happen even with further increases in dosage. In toxicity studies, thresholds are the critical points up to which cells can still repair damage and detoxify the exposed chemicals. The threshold dose is normally used for determining a no observable adverse effect level (NOAEL), which is essential for assigning the safety levels. The dose-response curve is normally sigmoidal with the steepest slope in the middle. The EC<sub>50</sub> (half-maximal effective concentration) or IC<sub>50</sub> (half-maximal inhibitory concentration) point is defined as the inflection point of the curve. Knowledge of the dose-response relationship allows one to

determine the thresholds for the adverse effects and the rates of building up these effects at increasing dose levels. The exposure conditions, related to patterns of response of host, include routes of exposure, frequency and duration of exposure, mixed exposures and environmental circumstances. Toxic agents may damage any contacted cells or affect only specific target organs. The effects vary depending on the dosage and route of exposure. Toxicity can result from cellular or biochemical changes, including cell replacement (e.g. fibrosis), damage to an enzyme system, disruption of protein synthesis, production of reactive chemicals in cells, and DNA damage.

A large number of environmental agents and drug candidates require fast and efficient *in vitro* toxicological risk assessments. Quantitative HTS (qHTS) has been adapted as a useful tool for toxicity testing, offering the benefits of reducing cost and restricting the number of the laboratory animals needed.<sup>33</sup> Developing a selective and sensitive approach for *in vitro* toxicity testing can effectively eliminate the false negatives—incapability of discerning the chemicals that were little concerned from those with the greatest likelihood of having an adverse effect.<sup>34</sup> However, limited knowledge of mechanisms for many types of toxicity has made it difficult to design suitable *in vitro* toxicity testing assays. As a result, a set of target-specific assays were generally applied in the toxicity assessments, but the outcomes were still not satisfying.<sup>35</sup> Developing a selective and sensitive approach for *in vitro* bioactivity screening is a critical goal in toxicology studies. Multichannel FP-AuNPs sensors capable of generating specific patterns at low doses may provide more insights on the modes of actions and facilitate the elimination of the false negatives in the toxicity assessment.

## 1.2 Results and Discussions

### 1.2.1 Fabrication of a triple-channel fluorescent protein-gold nanoparticle sensor

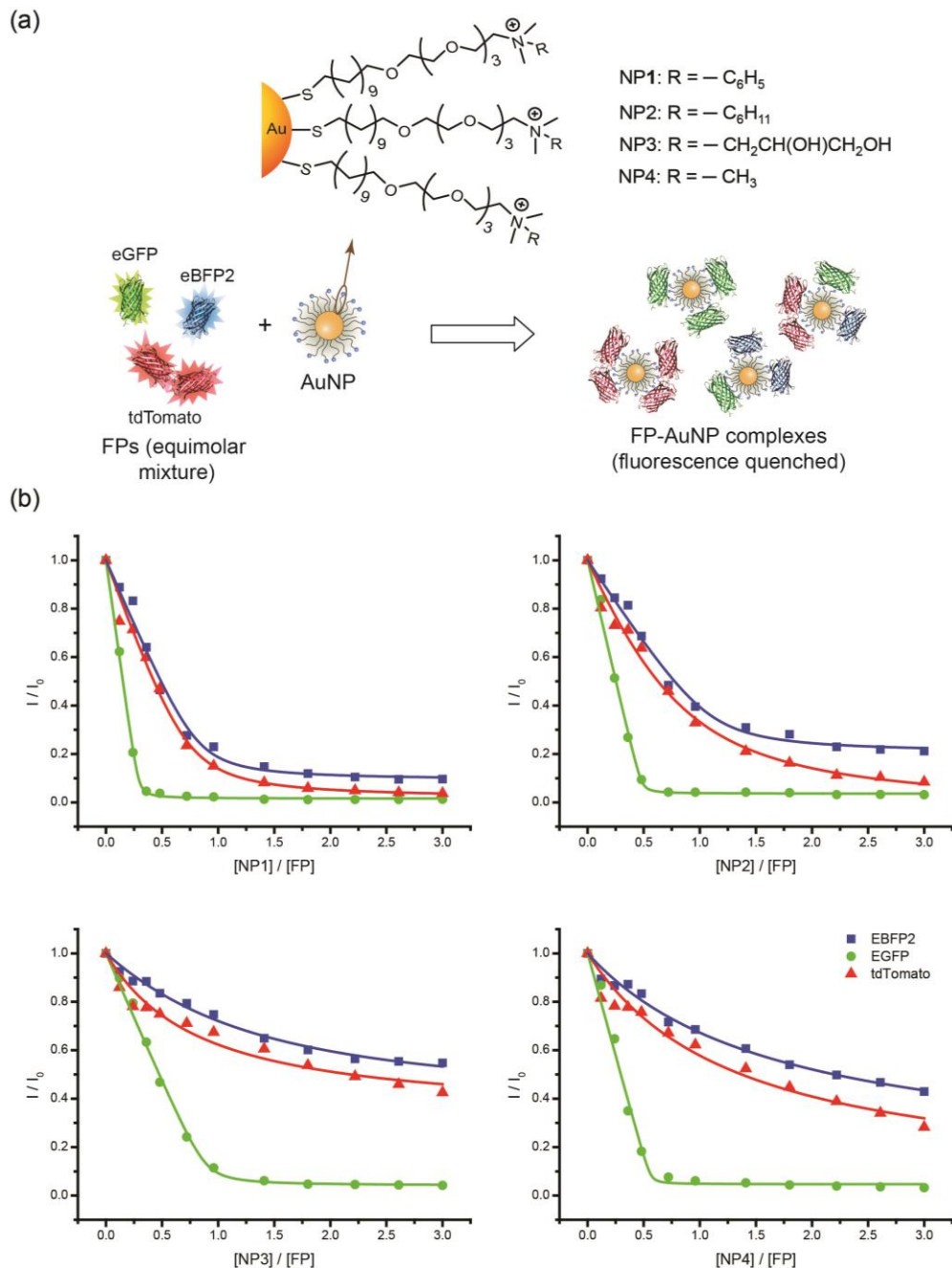


**Figure 1.8** (a) Schematic of the FP-AuNP complex formation and structures of the cationic AuNPs (NP1-NP5). (b) The scheme of triple-channel FP-AuNP complexes and fluorescence titration curves for 100 nM FPs with four different cationic AuNPs (NP1-NP4). The changes of fluorescence intensity were measured following the addition of AuNPs at 25<sup>0</sup>C. The solid lines represent the best curve fitting using Equation 1.1.

**Table 1.1** Binding constant ( $K_b$ ) and binding stoichiometry ( $n$ ) between FP and AuNPs (NP1-NP4) as determined from the fluorescence titrations.

Type of AuNP	Fluorescent Protein	Binding constant ( $K_b$ ), $nM^{-1}$	Binding Ratio ( $n$ )	$R^2$
NP1	EBFP2	0.26	1.21	0.9885
	EGFP	1.36	3.42	0.9990
	tdTomato	0.14	1.35	0.9882
NP2	EBFP2	0.20	0.92	0.9906
	EGFP	3.49	2.07	0.9940
	tdTomato	0.026	1.34	0.9867
NP3	EBFP2	0.014	1.58	0.9875
	EGFP	1.01	1.12	0.9965
	tdTomato	–	–	–
NP4	EBFP2	–	–	–
	EGFP	5.21	1.78	0.9902
	tdTomato	–	–	–

The triple-channel fluorescent protein-gold nanoparticle sensor is formed by cationic headgroup terminated AuNP mixed with three FPs, EBFP2 (pI 6.3,  $\lambda_x/\lambda_m$  383/448 nm), EGFP (pI 6.0,  $\lambda_x/\lambda_m$  488/507 nm), and tdTomato (pI 6.4,  $\lambda_x/\lambda_m$  550/585 nm). To investigate the appropriate headgroup of AuNPs for multichannel biosensing, several previously used AuNPs were titrated with the equimolar FP mixture. The fluorescent titration curves were fitted by the following binding model<sup>36</sup>:

$$I = I_0 + \frac{\alpha}{2} \left[ \left( [FP]_0 + n[AuNP]_{tot} + \frac{1}{K_b} \right) - \left\{ \left( [FP]_0 + n[AuNP]_{tot} + \frac{1}{K_b} \right)^2 - 4n[FP]_0[AuNP]_{tot} \right\}^{\frac{1}{2}} \right] \quad (1.1)$$

In this equation,  $I_0$  is the initial fluorescence intensity,  $I$  is the fluorescence intensity after addition of the quencher (AuNP),  $[FP]_0$  represents the initial concentration of the fluorescent signal producer (FP),  $[AuNP]_{tot}$  represents the total concentration of AuNPs,

$K_b$  is the binding constant (or the Stern-Volmer constant), and  $n$  denotes the number of binding sites around the AuNPs. The condition of applying this equation is  $K_b[FP]_0 \gg 1$ . NP1 and NP2 showed high binding affinities and different responses to three fluorescent proteins. (Figure 1.8 and Table 1.1)

Furthermore, to verify the classification capability of multichannel sensors, FP-NP1 and FP-NP2 complexes were individually applied to identify 2.5 nM proteins (fibrinogen, IgG,  $\alpha$ -antitrypsin, holo-transferrin) in a 200 fold diluted fetal bovine serum (FBS) solution. By LDA, FP-NP1 showed 75% accuracy in the jackknifed classification matrix. However, using the same procedure, NP2 showed only 46% accuracy. The most significant canonical factors that represent linear combinations of the response matrices obtained from the fluorescence-response patterns (three fluorescent signals  $\times$  four proteins  $\times$  six replicates) were plotted in two dimensions (Figure 1.9). Therefore, the triple channel FP-NP1 sensor is more promising for chemical nose sensing and applied for the following sensing process.

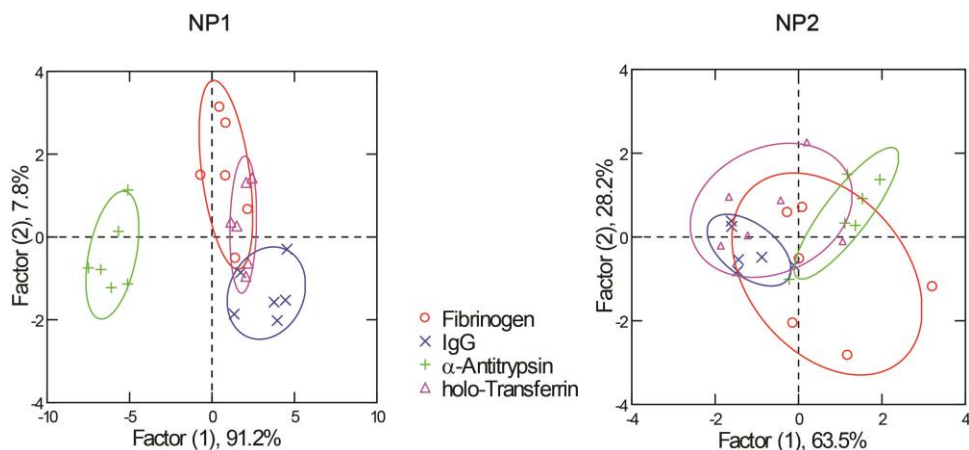


**Figure 1.9** Canonical score plots for the fluorescence patterns as obtained from LDA against four protein analytes spiked in FBS at fixed concentration (2.5 nM) with 95% confidence ellipses.

## 1.2.2 Cytotoxicity testing of drugs by viability assays

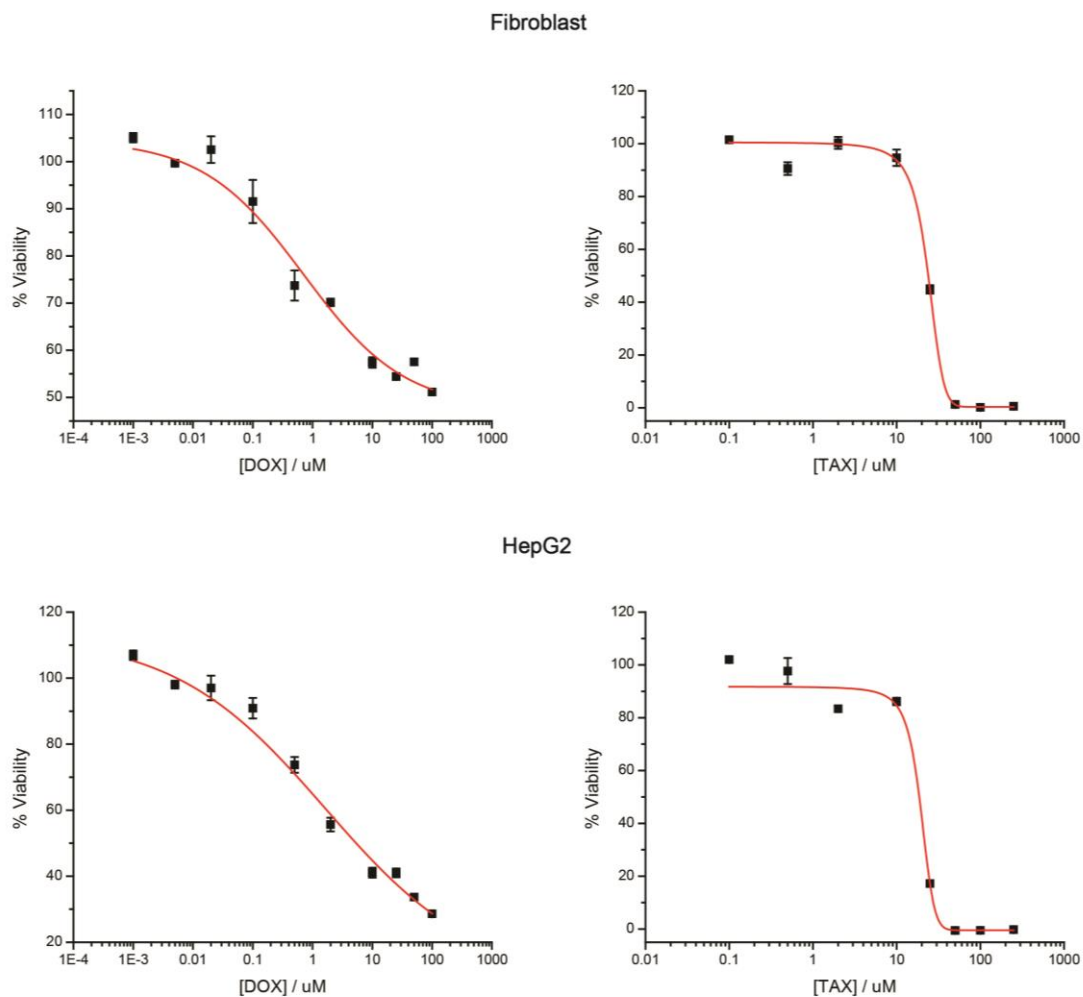


**Figure 1.10** Dose-response curves of DOX and TAM obtained by alamar blue assay, using 7,500 cells per well after 24 hours of drug treatments.

Before evaluating the cell changes at various doses by triple channel FP-NP1 sensors, the cytotoxicity of the chemicals was first tested by a conventional method, alamar blue assay. Two chemicals were selected: Doxorubicin (DOX), a topoisomerase II inhibitor targeting DNA replication process<sup>37</sup>, and Tamoxifen (TAM), a selective estrogen receptor modulator blocking cancer cell growth<sup>38</sup>. Both of these two chemicals induce the apoptotic mode of the cell death. For the purpose of toxicity studies, human hepatocellular carcinoma

cells (HepG2) and human newborn foreskin fibroblast cells were selected. The threshold dose, IC<sub>10</sub>, IC<sub>30</sub>, and IC<sub>50</sub> values were carried out after 24 hours exposure to these chemicals (Figure 1.10 and Table 1.2). To obtain these values, the dose-response curves were fitted to the Hill equation.<sup>39</sup>

**Table 1.2** Threshold doses and IC values obtained from dose-response curves fitted to the Hill equation.

Cell line	Drugs	Threshold dose	IC <sub>10</sub>	IC <sub>30</sub>	IC <sub>50</sub>
<b>Fibroblast</b>	DOX / uM	0.006	0.09	1.6	100
	TAM / uM	1.6	12	19	24
<b>HepG2</b>	DOX / uM	0.005	0.04	0.56	5.3
	TAM / uM	0.5	5.1	15	19

### 1.2.3 Unbiased sensing at varied doses using multichannel sensors

IC<sub>50</sub>s have been used to categorize the mechanism of actions of chemotherapeutic drugs with BT549 cell line.<sup>31</sup> For these two drugs, fluorescent signal patterns generated by triple channel FP-NP1 sensors could further illustrate the cellular responses related to the relative mechanisms of actions at low drug doses (Figure 1.11). It is noticeable that at the threshold dose, HepG2 showed higher fluorescent intensities when exposed to TAM than to the control (1% DMSO), which means that cells had undergone proliferation rather than death. This effect is called hormesis, and will be further discussed in the Chapter 2. This interesting finding implies that in order to determine *in vitro* NOAEL, additional bioassays should be applied to evaluate the response around the threshold dose and multichannel FP-NP1 sensors could be a powerful tool.

By LDA, the fluorescence patterns at thresholds, IC<sub>10</sub>s, and IC<sub>30</sub>s can be easily characterized to classify the activities of the cells at these doses. For fibroblast, the clusters

at respective doses of these two drugs (thresholds or different ICs), always partially overlap with each other, which implies the similarity on the cell responses. In contrast, for HepG2, the clusters at either thresholds or different ICs, are well separated for these two drugs, which means that there may be two distinct mechanisms of actions. For the same cell line and drug, the separation of clusters among different doses also reveals the effects of doses on the cell responses.

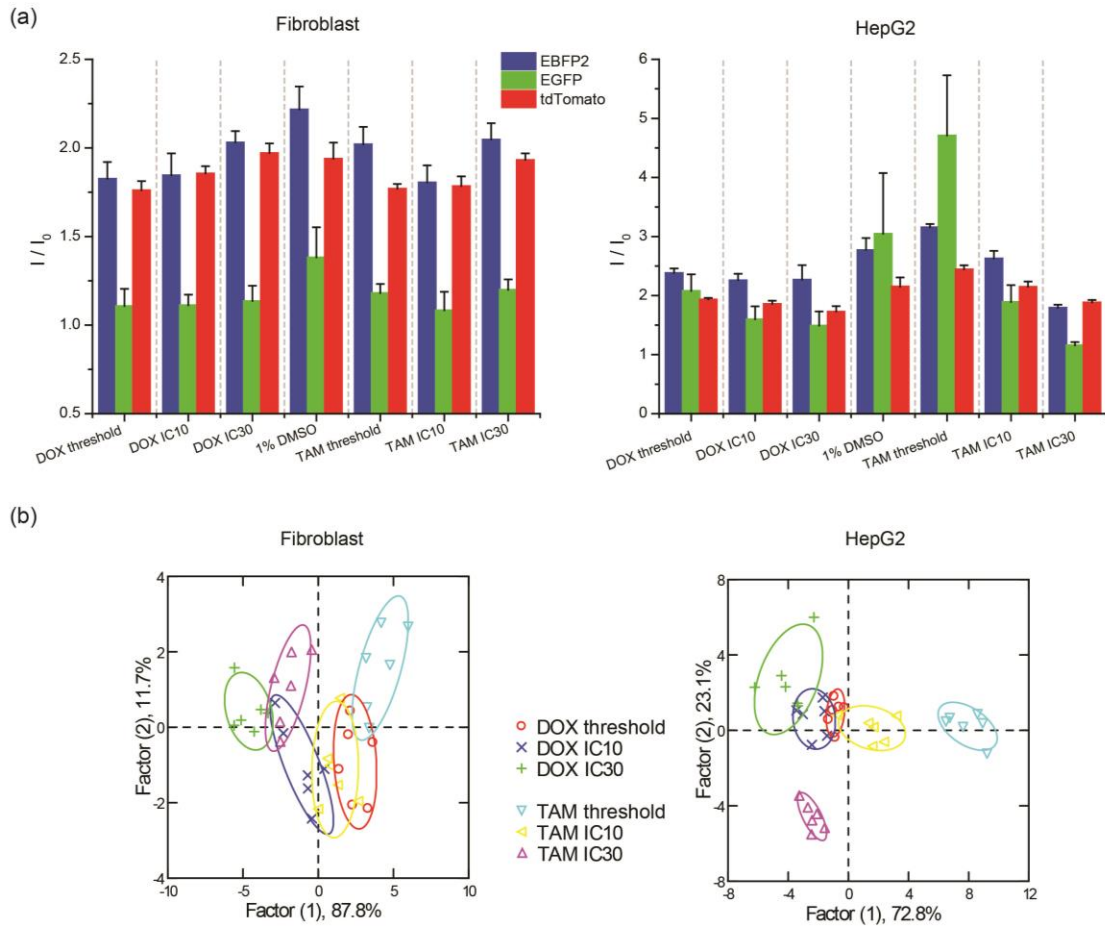


**Figure 1.11** Differentiation of cell responses to DOX and TAM at three low doses (threshold doses,  $IC_{10}$ s, and  $IC_{30}$ s). (a) Changes in fluorescence intensities (mean of six replicates) for two cell lines treated with DOX or TAM individually (control in 1% DMSO). (b) Canonical plots of discriminant scores with 95% confidence ellipses for all data points.

### **1.3 Conclusions**

An unbiased triple channel sensor comprised of triple channel FPs and NP1 was presented to identify the cell responses exposed at low doses. The results demonstrate the power of triple channel FP-NP1 sensor in evaluating the cell responses around threshold doses and classifying the cell specific modes of actions in *in vitro* toxicity testing. As a candidate of cell-based HTS, this method can accelerate the testing procedure and eliminate the possibility of false negatives in toxicity assessments.

### **1.4 Experimental Methods**

#### **1.4.1 Expression and purification of fluorescent proteins**

EBFP2, EGFP and tdTomato genes were reconstructed into pQE80 plasmid. *E. coli* BL21 (DE3) strain was transformed with the respective plasmids. The culture grew in LB media at 37°C until OD reaches 0.6. After the overnight induction of IPTG at 25°C, cells were harvested and the pellets were lysed using lysozyme. The fluorescent proteins in the lysed supernatant were purified using HisPur Cobalt columns. The purified proteins were dialyzed in 5 mM sodium phosphate buffer (pH 7.4). The purity and concentration were determined by SDS-PAGE and absorbance spectroscopy.

#### **1.4.2 Fluorescence titrations and protein sensing**

In fluorescence titration experiments, the NPs were titrated into 100 nM equimolar FPs in sodium phosphate buffer (pH 7.4). The changes of fluorescence intensities at 450 nm, 510 nm and 585 nm, were measured on a Molecular Devices SpectraMax M3

microplate reader at 25<sup>0</sup>C with excitation wavelengths of 380 nm, 475 nm and 550 nm, respectively.

For serum protein sensing, 5 uL proteins spiked in diluted FBS were added into 200 uL FP-AuNP solutions on a 96-well plate. After incubation of 30 minutes, the fluorescence intensities were measured using the same method in the previous titration experiment. The data matrix was processed by LDA using SYSTAT software.

### **1.4.3 Threshold doses, IC<sub>10S</sub>, IC<sub>30S</sub> determination**

Fibroblastic and HepG2 cells were seeded at 7500 cells / well in 96-well plates 24 hours prior to the drug treatments. After the addition of DOX and TAM (in 1% DMSO) for 24 hours, the cells were washed twice with PBS and treated with 10% alamar blue in serum-containing media for 3 hours. The substrate fluorescence intensity was read at 535/590 nm ( $\lambda_x / \lambda_m$ ). The dose-response curves were fitted to the Hill equation, yielding threshold doses, IC<sub>10S</sub>, IC<sub>30S</sub> and IC<sub>50S</sub>.

### **1.4.4 Cell sensing studies using multichannel sensors**

After being treated with DOX and TAM at threshold doses, IC<sub>10S</sub>, and IC<sub>30S</sub>, HepG2 and fibroblastic cells were carefully washed by PBS buffer twice and 200 uL triple channel FP-NP1 sensors were added. After half an hour, the plates were read through the plate reader (at 25<sup>0</sup>C). The results were analyzed by LDA.

## 1.5 References

1. Stoeva, S. I.; Lee, J.-S.; Thaxton, C. S.; Mirkin, C. A. *Angewandte Chemie International Edition* **2006**, *45*, 3303–3306.
2. You, C.-C.; Miranda, O. R.; Gider, B.; Ghosh, P. S.; Kim, I.-B.; Erdogan, B.; Krovi, S. A.; Bunz, U. H. F.; Rotello, V. M. *Nature Nanotechnology* **2007**, *2*, 318–323.
3. Bajaj, A.; Rana, S.; Miranda, O. R.; Yawe, J. C.; Jerry, D. J.; Bunz, U. H. F.; Rotello, V. M. *Chemical Science* **2010**, *1*, 134–138.
4. Shipway, A. N.; Katz, E.; Willner, I. *ChemPhysChem* **2000**, *1*, 18–52.
5. Anker, J. N.; Hall, W. P.; Lyandres, O.; Shah, N. C.; Zhao, J.; Van Duyne, R. P. *Nat Mater* **2008**, *7*, 442–453.
6. Sheehan, P. E.; Whitman, L. J. *Nano Lett.* **2005**, *5*, 803–807.
7. Saha, K.; Agasti, S. S.; Kim, C.; Li, X.; Rotello, V. M. *Chemical Reviews* **2012**, *112*, 2739–2779.
8. Su, K.-H.; Wei, Q.-H.; Zhang, X.; Mock, J. J.; Smith, D. R.; Schultz, S. *Nano Lett.* **2003**, *3*, 1087–1090.
9. Elghanian, R.; Storhoff, J. J.; Mucic, R. C.; Letsinger, R. L.; Mirkin, C. A. *Science* **1997**, *277*, 1078–1081.
10. Rosi, N. L.; Mirkin, C. A. *Chem. Rev.* **2005**, *105*, 1547–1562.
11. Daniel, M.-C.; Astruc, D. *Chem. Rev.* **2004**, *104*, 293–346.
12. Greene, N. T.; Shimizu, K. D. *J. Am. Chem. Soc.* **2005**, *127*, 5695–5700.
13. You, C.-C.; De, M.; Rotello, V. M. *Org. Lett.* **2005**, *7*, 5685–5688.
14. De, M.; You, C.-C.; Srivastava, S.; Rotello, V. M. *J. Am. Chem. Soc.* **2007**, *129*, 10747–10753.
15. Bayraktar, H.; Ghosh, P. S.; Rotello, V. M.; Knapp, M. J. *Chem. Commun.* **2006**, 1390–1392.
16. De, M.; Rana, S.; Akpınar, H.; Miranda, O. R.; Arvizo, R. R.; Bunz, U. H. F.; Rotello, V. M. *Nature Chemistry* **2009**, *1*, 461–465.
17. Rana, S.; Singla, A. K.; Bajaj, A.; Elci, S. G.; Miranda, O. R.; Mout, R.; Yan, B.; Jirik, F. R.; Rotello, V. M. *ACS Nano* **2012**, *6*, 8233–8240.

18. Phillips, R. L.; Miranda, O. R.; You, C.-C.; Rotello, V. M.; Bunz, U. H. F. *Angewandte Chemie International Edition* **2008**, *47*, 2590–2594.
19. Bajaj, A.; Miranda, O. R.; Phillips, R.; Kim, I.-B.; Jerry, D. J.; Bunz, U. H. F.; Rotello, V. M. *Journal of the American Chemical Society* **2010**, *132*, 1018–1022.
20. Elci, S. G.; Moyano, D. F.; Rana, S.; Tonga, G. Y.; Phillips, R. L.; Bunz, U. H. F.; Rotello, V. M. *Chemical Science* **2013**, *4*, 2076.
21. Gnanadesikan, R. *Discriminant Analysis and Clustering*; National Academies Press, 1988.
22. Zhang, R.; Beyer, B. M.; Durkin, J.; Ingram, R.; Njoroge, F. G.; Windsor, W. T.; Malcolm, B. A. *Analytical Biochemistry* **1999**, *270*, 268–275.
23. Lowery, R. G.; Kleman-Leyer, K. *Expert Opinion on Therapeutic Targets* **2006**, *10*, 179–190.
24. Carmody, L. C.; Germain, A. R.; VerPlank, L.; Nag, P. P.; Muñoz, B.; Perez, J. R.; Palmer, M. *J Biomol Screen* **2012**, 1087057112458317.
25. Bandyopadhyay, S.; Ni, J.; Ruggiero, A.; Walshe, K.; Rogers, M. S.; Chattopadhyay, N.; Glicksman, M. A.; Rogers, J. T. *J Biomol Screen* **2006**, *11*, 469–480.
26. Inglese, J.; Johnson, R. L.; Simeonov, A.; Xia, M.; Zheng, W.; Austin, C. P.; Auld, D. S. *Nature Chemical Biology* **2007**, *3*, 466–479.
27. Eglén, R. M.; Bosse, R.; Reisine, T. *ASSAY and Drug Development Technologies* **2007**, *5*, 425–452.
28. Reichling, L. J.; Lebakken, C. S.; Riddle, S. M.; Vedvik, K. L.; Robers, M. B.; Kopp, L. M.; Bruinsma, R.; Vogel, K. W. *J Biomol Screen* **2008**, *13*, 238–244.
29. Huang, R.; Xia, M.; Cho, M.-H.; Sakamuru, S.; Shinn, P.; Houck, K. A.; Dix, D. J.; Judson, R. S.; Witt, K. L.; Kavlock, R. J.; Tice, R. R.; Austin, C. P. *Environ Health Perspect* **2011**, *119*, 1142–1148.
30. Zheng, W.; Spencer, R. H.; Kiss, L. *ASSAY and Drug Development Technologies* **2004**, *2*, 543–552.
31. Rana, S. Effective biosensor arrays using gold nanoparticle-protein conjugates. Ph.D., University of Massachusetts Amherst: United States -- Massachusetts, 2013.
32. Klaassen, C. *Casarett & Doull's Toxicology: The Basic Science of Poisons, Eighth Edition (Casarett & Doull's Toxicology)*; 8 edition.; McGraw-Hill Professional, 2013.

33. Xia, M.; Huang, R.; Witt, K. L.; Southall, N.; Fostel, J.; Cho, M.-H.; Jadhav, A.; Smith, C. S.; Inglese, J.; Portier, C. J.; Tice, R. R.; Austin, C. P. *Environ Health Perspect* **2008**, *116*, 284–291.
34. Dix, D. J.; Houck, K. A.; Martin, M. T.; Richard, A. M.; Setzer, R. W.; Kavlock, R. J. *Toxicol. Sci.* **2007**, *95*, 5–12.
35. Schoonen, W. G. E. J.; Westerink, W. M. A.; Horbach, G. J. In *Molecular, Clinical and Environmental Toxicology*; Luch, A., Ed.; Experientia Supplementum; Birkhäuser Basel, 2009; pp. 401–452.
36. Bunz, U. H. F.; Rotello, V. M. *Angewandte Chemie International Edition* **2010**, *49*, 3268–3279.
37. King, P. D.; Perry, M. C. *The Oncologist* **2001**, *6*, 162–176.
38. Majumdar, S. K.; Valdellon, J. A.; Brown, K. A. *J Biomed Biotechnol* **2001**, *1*, 99–107.
39. Gesztelyi, R.; Zsuga, J.; Kemeny-Beke, A.; Varga, B.; Juhasz, B.; Tosaki, A. *Arch. Hist. Exact Sci.* **2012**, *66*, 427–438.

## CHAPTER 2

### CELL-BASED SENSING OF ENDOCRINE DISRUPTING CHEMICALS USING GREEN FLUORESCENT PROTEIN-GOLD NANOPARTICLE COMPLEXES

#### 2.1 Introduction

##### 2.1.1 Hormones and endocrine disrupting chemicals

Steroid hormones are a class of regulatory biomolecules that play a central role in the control of a variety of physiological and behavioral activities, including metabolism, tissue function, sensory perception, growth and development, reproduction, stress and mood.<sup>1</sup> Estradiol (E2 or 17 $\beta$ -estradiol), the principle hormone, is derived from cholesterol and synthesized by testosterone aromatization (Figure 2.1).<sup>2</sup> The aromatase enzymes can be found in many tissues, including brain, skin, blood vessels, and even breast cancer tumors.<sup>3</sup> E2 can passively diffuse through the cell plasma membrane and interact with cytoplasmic hormone-specific estrogen receptors (ERs). After activated by E2, dimeric ERs translocate into the nucleus and bind to estrogen response elements (EREs) on DNA sequences to regulate the expression of specific genes. ER is a member of the nuclear receptor (NR) superfamily of estrogen receptor-like, also including the androgen receptor (AR), progesterone receptor (PR), mineralcorticoid receptor (MR), and glucocorticoid receptor (GR).<sup>4</sup> ERs include ER $\alpha$ , ER $\beta$  and G-protein-coupled estrogen receptor 1 (GPER).<sup>5</sup> ER $\alpha$  and ER $\beta$  can form homodimers or heterodimers and exhibit distinct transcriptional properties.

Endocrine disrupting chemicals (EDCs) are compounds, either natural or synthetic, which interfere with endocrine systems through environmental or inappropriate developmental exposures and produce adverse health effects in both human and wildlife,

such as the development of hormone-dependent cancers, disorders of the reproductive tract, obesity and reduction of sperm counts.<sup>6</sup> EDCs represent a broad class of molecules, including environmental pollutants and industrial chemicals, such as pesticides and thermoplastics<sup>7</sup>.

Bisphenol A (BPA) is used in the production of polycarbonate and epoxy resins, which are widely coated on the inside of food and beverage cans. (Figure 2.1) BPA, as an example of EDCs, has been shown to mediate ER activity in a number of *in vitro* and *in vivo* assays.<sup>8</sup> Known as a potential hazard to infants and young children, BPA usage was banned in baby bottles and infant formula packaging.

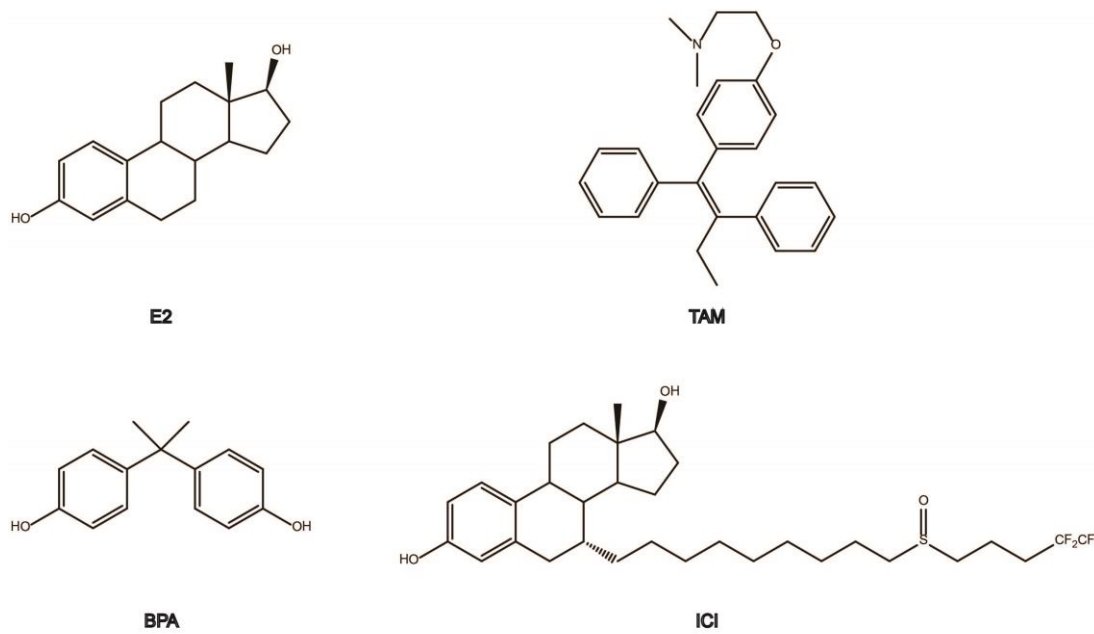


**Figure 2.1** Structures of selective and nonselective ER ligands. Compounds shown include E2 (nonselective activators), TAM (selective ER modulator), xenoestrogen BPA, and a selective ER downregulator ICI 182,780 (ICI).

## 2.1.2 The cellular estrogen signaling pathways

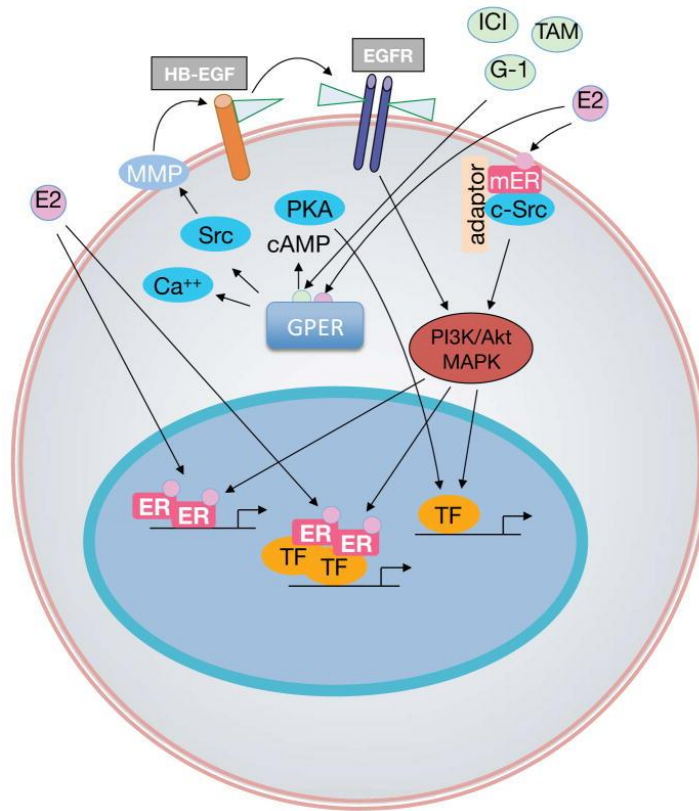


**Figure 2.2** Schematic model illustrating genomic and non-genomic estrogen signaling pathways. E2 activates ER $\alpha$  and ER $\beta$ , inducing dimerization and binding to the promoters of target genes. Alternatively, other classes of TFs (transcription factors) can also be modulated by activated ERs. A small population of activated ERs at the plasma membrane (mER) interact with adaptor proteins and signaling molecules such as c-Src, and regulate rapid (non-genomic) effects or gene transcription via PI3K/AKT (phosphatidylinositol 3-kinase/protein kinase B) and MAPK (mitogen-activated protein kinase) pathways. E2, or selective ER ligands (such as G-1, ICI, and TAM), can activate intracellular GPER, which stimulates cAMP production, calcium mobilization and c-Src, which activates MMPs (matrix metalloproteinases). MMPs cleave pro-HB-EGF (pro-heparin-binding-epidermal growth factor), releasing free HB-EGF that transactivates EGFR (EGF receptor), which also in turn activates PI3K/AKT and MAPK pathways. (Ref. 5)

E2 regulates human physiology via two types of cellular signaling pathways, genomic and non-genomic pathways (Figure 2.2).<sup>2,5</sup> ER $\alpha$  and ER $\beta$  are encoded by different genes located on different chromosomes, yet sharing high sequence homology. There are

several common regions, mainly including the DNA binding domain (DBD), ligand binding domain (LBD), and hinge domain. DBD allows the dimerization of ERs and binds to ERE sequences through zinc finger structures. LBD contains the E2 binding domain and regulates the gene transcription with co-activators. The hinge domain (D domain) plays a role in ER dimerization and binding to chaperone heat-shock proteins (Figure 2.3).

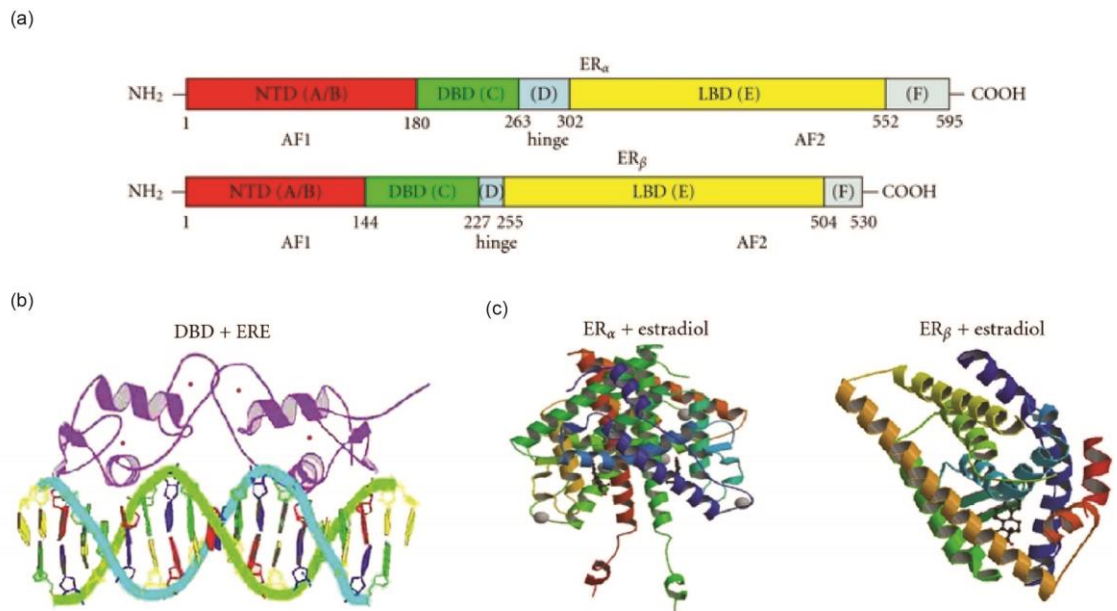


**Figure 2.3** (a) Domain organization of ER $\alpha$  and ER $\beta$ . ERs consist of N-terminal domain (NTD, in red), DNA binding domain (DBD, in green), the hinge region (D domain, in blue), ligand binding domain (LBD, in yellow), and C-terminal end (in grey). (b) Binding mode of ERE to dimeric ER $\alpha$  (PDB: 1HCQ) (c) Structures of ER $\alpha$  and ER $\beta$  bound to E2 (PDB: 1A52 and 3OLS). (Ref. 9)

There are direct and indirect action modes in the genomic pathways. The direct action mode has been described previously, in which an ERE-like sequence should be constructed within the promoter. However, without any ERE-like sequences, a second DNA-binding transcription factor is needed to mediate ER indirect association with DNA. ER $\alpha$  and ER $\beta$  are shown to signal in opposite ways through interaction with different co-

regulators. For example, in the presence of E2, ER $\alpha$  enhances the binding of specificity protein-1 (Sp-1) in GC-rich regions to increase the transcription of a number of genes, such as the low-density lipoprotein (LDL) receptor and cyclin D1, but ER $\beta$  cannot form any transcriptionally active complex at the promoter region.<sup>2</sup> The differences in their transcriptional activities may result in their tissue specific biological actions.

The genomic action of E2 occurs after a time-lag of at least 2 hours after stimulation, and however, ER-E2 complexes can activate non-genomic pathways, such as the process of kinase-dependent phosphorylation, rapidly within minutes<sup>10</sup>. There are a subpopulation of ERs located at the plasma membrane. The conformation changes of ER LBD domain after the stimulus of E2, allow ER-E2 complexes to interact with adapter proteins to activate the downstream signaling pathways. Rapid signaling through GPER occurs via transactivation of EGFR, involving nonreceptor tyrosine kinases of the Src family, MMP and HB-EGF. (Figure 2.2) Non-genomic signals mediate cell-specific functions, such as proliferation effects and neural functions.

### **2.1.3 Low dose effects and non-monotonic dose responses**

From the National Toxicology Program's (NTP) peer review of the low-dose EDC in 2001, low dose effects are defined as biological changes occurring in the range of environmentally relevant exposure levels or at a dose lower than those typically used in the U.S. Environmental Protection Agency's (EPA) standard toxicity testing protocols.<sup>11</sup> There are different low dose cut-offs for the environmental exposure level and traditional toxicology assays. As an example, the low dose cut-off of BPA was set at 100 nM (~ 0.02 mg/L) for *in vitro* studies and 17.2 mg/L for aquatic animals.<sup>12</sup> A large number of studies

have shown that at or below the low dose cut-off the endocrine disrupting activities still exist. As potential adverse health threaten to human, low dose effects should receive more

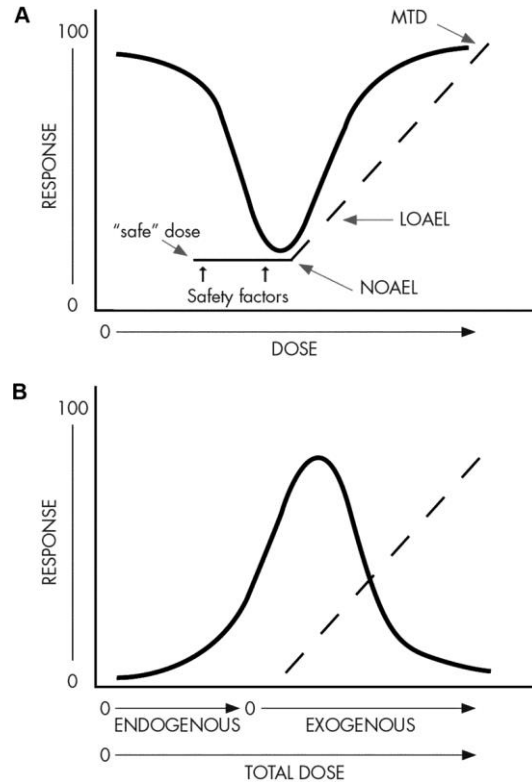


**Figure 2.4** Examples of NMDRCs. High doses (shown by dotted line) are tested to obtain the maximum tolerated dose (MTD), the lowest observed adverse effect level (LOAEL), and NOAEL. Safety factors are applied to derive the “safe” dose. However, in the actual dose-response curves, U-shaped (A) and inverted U-shaped (B) NMDRCs shown by solid lines, the adverse effects may be observed below the “safe” dose. B represents the response of EDCs. Both endogenous and exogenous effects are present. No dose in this range can be considered safe. (Ref. 8)

attention.

Non-monotonic dose response curves (NMDRCs) are found in EDC studies.<sup>8</sup> Typically, the monotonic dose response curve, linear or nonlinear, refers to a greater response in the test as the dose increases. However, the slope of the NMDRC changes the sign at some point within the range of doses. It is usually a U-shaped or inverted U-shaped

curve. The existence of NMDRCs means that the high dose toxicity assessments cannot predict the safety at lower doses, perhaps leading to false negatives (Figure 2.4).

Low dose effects of EDCs should be distinguished from hormesis, a non-monotonic or biphasic dose response, which typically refers to the low-dose beneficial and high-dose detrimental pattern under the biological and ecological context of the response (Figure 2.5).<sup>13</sup> One example of hormesis is that some anticancer drugs (e.g. TAM) can enhance the tumor cell proliferation at low doses.<sup>14</sup> The main issue of low dose effects is that it is still under debate how to define adverse health effects at the low-dose exposure of EDCs.

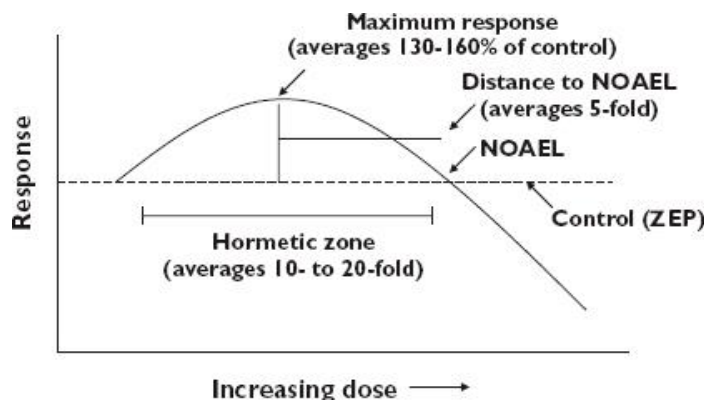


**Figure 2.5** A representative dose response curve indicating the quantitative features of hormesis. (Ref. 15)

#### 2.1.4 *In vitro* assays for assessing endocrine disrupting chemicals

*In vivo* assays assessing EDCs are not suitable for large-scale screening and limited due to the poor sensitivity, modest responsiveness and high cost. They utilize highly complex responses that may not directly involve ERs, and therefore cannot be selective to EDCs. As a comparison, *in vitro* assays are designed based on well elucidated mechanisms of actions of EDCs, which can be used to rapidly prioritize and identify estrogen-like properties of chemicals.<sup>16</sup>

The major *in vitro* assays for assessing the estrogenicity can be categorized into several groups: ER competitive ligand binding assays, cell proliferation assays (E-screen assays<sup>17</sup> or flow cytometric assays<sup>18</sup>), enzyme activity assays, reporter gene assays, and yeast-based assays.<sup>16</sup> As discussed previously, EDCs can have numerous impacts on gene expression, activities of transcription factors, and activations of signal transduction pathways. As a consequence, multitude of responses, such as cell growth, development, differentiation and homeostasis, may be elicited by the interplay between various mechanisms. There are limitations and potential problems of current *in vitro* assays, hence it is unrealistic to assume one assay is capable of predicting all the responses, and the assessments should be confirmed by other *in vitro* or *in vivo* assays. For example, endogenous promoter-regulated reporter gene assays are susceptible to the mechanisms that are not mediated by ERs, whereas they can provide high responsiveness and sensitivity.<sup>19</sup> Also, ERE-regulated reporter gene assays in which the introduction of the reporter gene only occurs through the ERE, exhibit a low responsiveness to the antagonist, in the presence of dextran-coated charcoal-treated fetal bovine serum (DCC-FBS).<sup>20</sup> For E-screen assays, long incubation period, discrepancies of estrogenicity identification using assays based on different cell lines, and interference by other NRs, may be a concern.<sup>21</sup> Despite these drawbacks, cell proliferation assays rarely report false positives and still one of the most sensitive *in vitro* assays to assess estrogenic activities.

As the requirement of testing the estrogenic activity of thousands of chemicals currently used in the United States, including the substances found in the drinking water and all the pesticides, an effective, responsive, and sensitive *in vitro* EDC screening assay should be developed.

## 2.2 Results and discussions

### 2.2.1 Cell viability tests by GFP-AuNP sensor and conventional methods

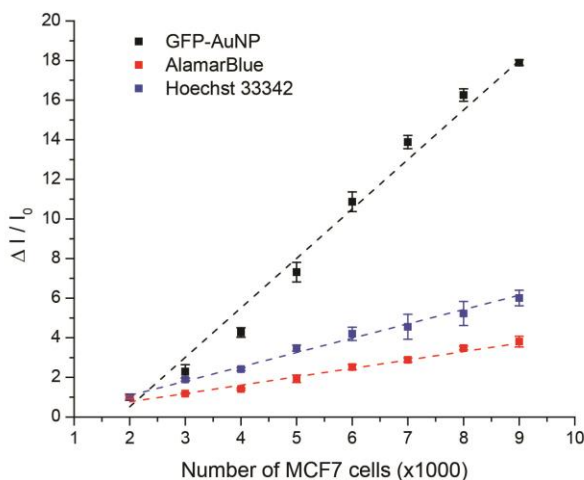


**Figure 2.6** The cell proliferation tests of MCF7 cells were performed by GFP-AuNP sensor, alamar blue reagent, and Hoechst 33342 stain. The dotted plots were linearly fitted.

As discussed previously, the cell proliferation assay, at present, is one of the most reliable assays in detecting EDCs, which implies that this sensing mechanism is effectively representative. Before applying the GFP-AuNP sensors to detect EDCs, its responsiveness to the cell proliferation should be investigated. Cationic benzyl headgroup gold nanoparticle is selected to fabricate the GFP-AuNP sensor due to its high binding affinity to GFP or even ERs potentially. Alamar blue and nuclear stain Hoechst 33342 are applied for comparison. The alamar blue reagent can be reduced by viable cells to indicate red fluorescence. Hoechst 33342 is a cell permeable stain, exhibiting distinct blue fluorescence after binding into the minor groove of DNA, which can be used to quantify DNA in solution. From 1k to 10k MCF7 cells per well on the 96-well plates, the slopes of the normalized

fluorescent intensity change plots show that the GFP-AuNP sensor is 3.5 times more responsive than Hoechst 33342 and 6 times than the alamar blue reagent. (Figure 2.6) Compared with alamar blue reagent, Hoechst 33342 stain does not interfere with FP-AuNP sensors and can be applied in the same well in the following sensing procedure.

### **2.2.2 Endocrine disrupting chemicals sensing using GFP-AuNP sensors**

The effects of E2 and BPA on the cell proliferation of growth arrested BT549, MCF7 and T47D were tested using the GFP-AuNP sensor and Hoechst 33342 stain after 24 hours incubation (Figure 2.7). To maintain the low steroid conditions before exposed to EDC containing media, DCC-FBS, phenol red free DMEM/F12 media, and phenol red free trypsin-EDTA solution were used. As a negative control, BT549 cell line, which lacks ERs, did not indicate any obvious cell proliferative responses to E2 or BPA with the GFP-AuNP sensor or Hoechst 33342 stain. Notably, MCF7 and T47D, both containing ERs, demonstrated clear dose responses to E2 and BPA by the GFP-AuNP sensor. In the presence of 10 nM ICI 182,780 (ICI), a strong antiestrogen, the proliferative effects of E2 and BPA were suppressed, which could also be shown by the GFP-AuNP sensor. For only 24 hours incubation of E2 and BPA, Hoechst 33342 was not responsive enough to clearly identify their estrogenic activities. The dose response curves were fitted by the Hill equation<sup>22</sup> to obtain EC<sub>50</sub>s and threshold doses (>15% of the maximum response, which is roughly equal to the SD value) (Table 2.1). For both MCF7 and T47D cell lines, the EC<sub>50</sub> values of E2 and BPA are less than 10<sup>-3</sup>-fold of the ones measured by E-screen assays.<sup>17,23</sup>

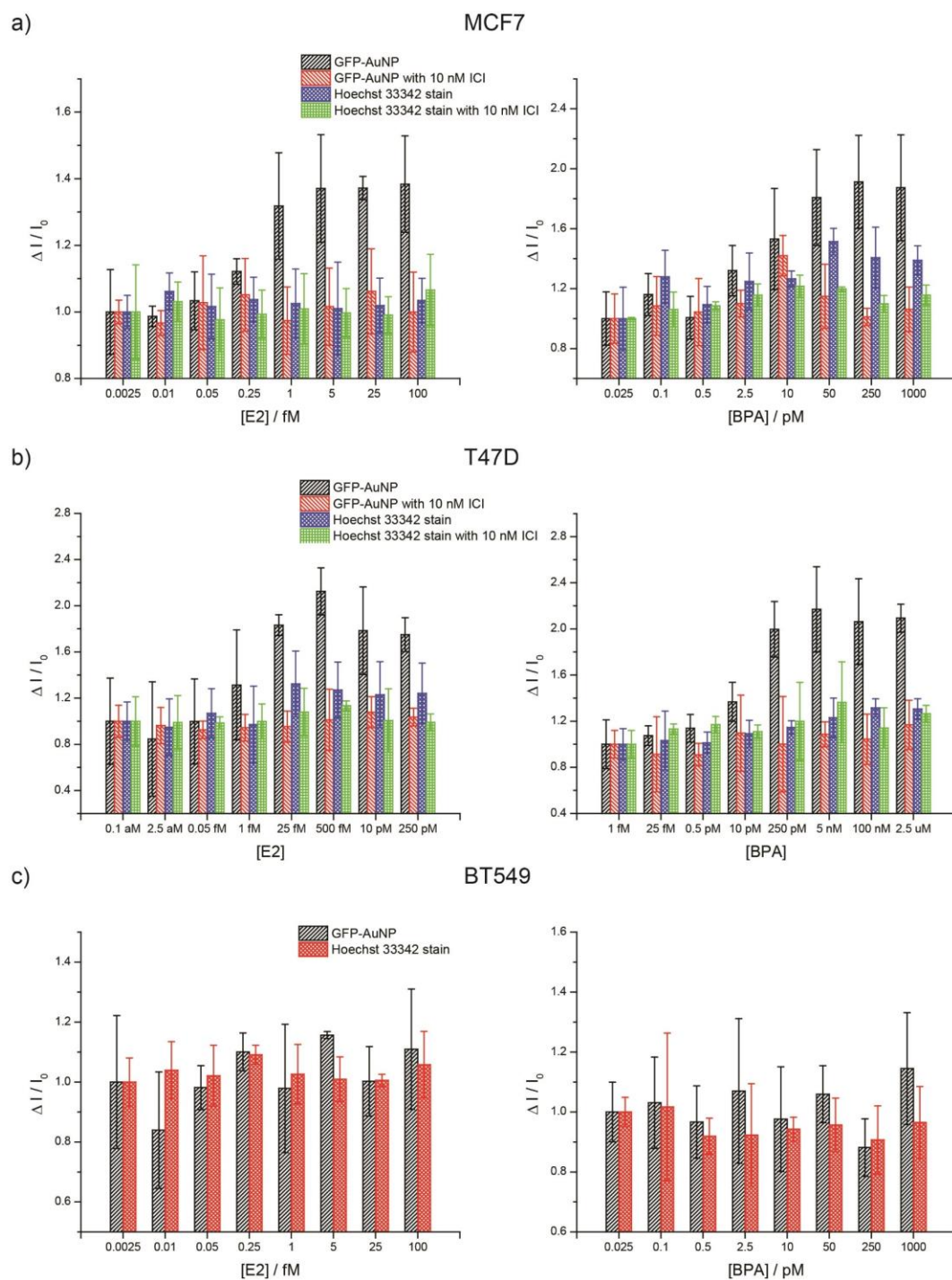


**Figure 2.7** Dose-response relationships of MCF7 (a), T47D (b) and BT549 (c) cell lines exposed to E2, BPA and ICI using GFP-AuNP sensor and Hoechst 33342 stain. Each value is the mean of three replicates.

Indicated by the GFP-AuNP sensor, the maximum responses of E2 and BPA on

MCF7 cell line remained constant at higher concentrations. However, for T47D cell line, responses slightly decreased when the concentrations of E2 or BPA increased, which indicates that NMDRCs may exist. Interestingly, with different lengths of E2 incubation time on MCF7 cell line, shapes of the dose response curves also varied. For 6 hour incubation, the cell proliferative effect appeared and the NMDRC was also demonstrated. 24 hour incubation produced the higher responses than 12 hour incubation at high doses (Figure 2.8). GFP-AuNP sensors are able to detect the cellular changes along the genomic estrogen signaling pathway.

**Table 2.1** The cell proliferation of MCF7 and T47D induced by E2 and BPA, were measured by GFP-AuNP sensor.

Cell line	EDCs	Threshold dose	EC <sub>50</sub>
MCF7	E2	0.11 fM	0.39 fM
	BPA	1.4 pM	5.7 pM
T47D	E2	0.33 fM	1.5 fM
	BPA	3.4 pM	26 pM

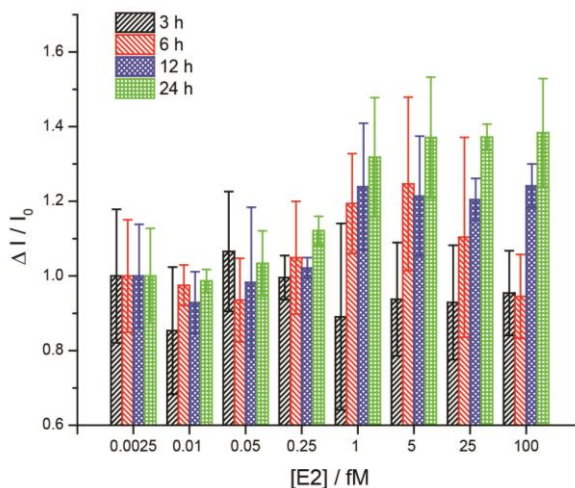


**Figure 2.8** Dose-response relationships of MCF7 cells at different exposure time of E2 were tested by GFP-AuNP sensor.

### 2.2.3 The mechanism of cell-based GFP-AuNP sensing strategy

Array-based GFP-AuNP methods can successfully identify and differentiate several types of mammalian cancer cells.<sup>24</sup> The essentials are the high sensitivity of GFP-AuNP sensors and the differences of glycan signatures on the cell surfaces effectively recognized by aromatic headgroup containing AuNPs. For the similar mechanism of actions of EDCs on the same cell line, changes of glycan signatures on the cell surface are subtle at different doses, and also, the enhancement of the DNA synthesis is not obvious by Hoechst 33342 stain (Figure 2.7). It is highly possible that the increased protein expression level is essential to the fluorescent change by GFP-AuNP sensors.

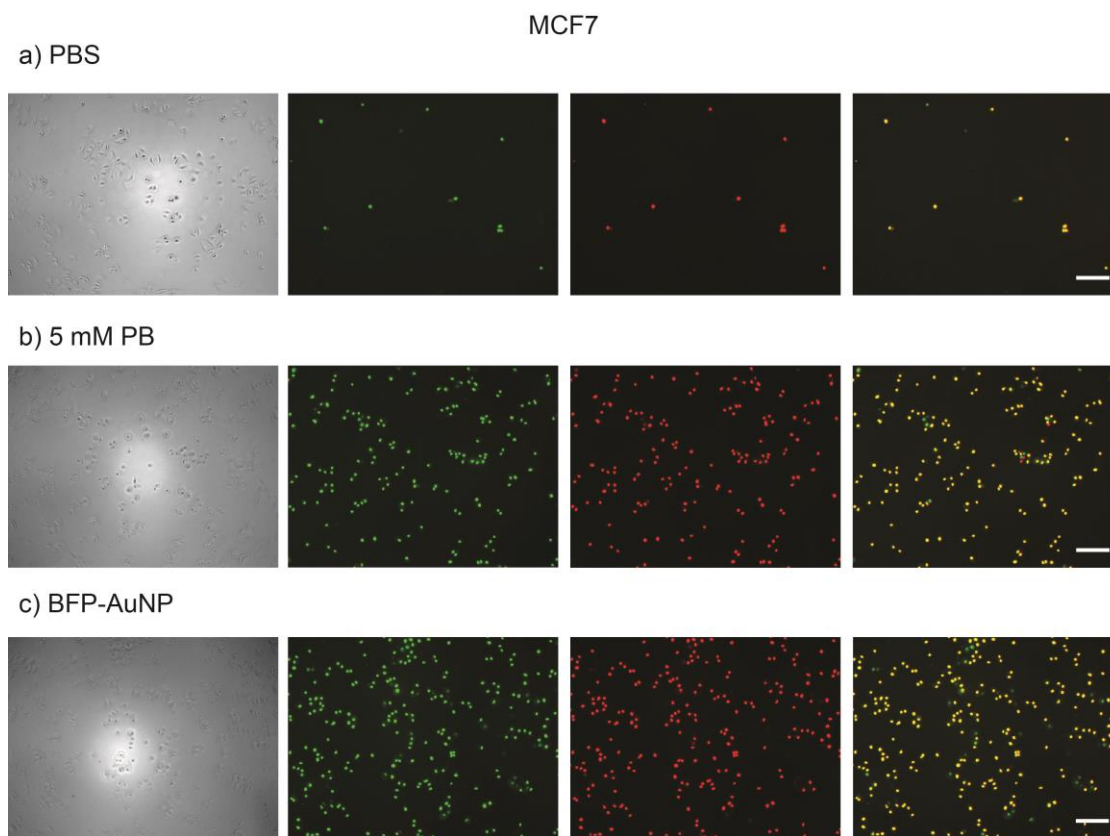


**Figure 2.9** Images of MCF7 cells stained by YO-PRO-1 (green fluorescence) and PI (red fluorescence) under different conditions: PBS buffer (a), 5 mM PB (pH 7.4) (b), and BFP-AuNP sensor in 5 mM PB (pH 7.4) (c). Scale bar: 200  $\mu$ m.

To investigate the sensing mechanism by GFP-AuNP sensors, fluorescent images were taken at different conditions (Figure 2.9). With nucleic acid stains YO-PRO-1 and propidium iodide (PI), the cell viabilities of MCF7 cells under different treatments were indicated. YO-PRO-1 stain is able to pass through the plasma membranes of apoptotic cells and labels them with green fluorescence. Necrotic cells are stained in red fluorescence by PI. After washed in PBS buffer, very few cells (~ 5%) showed apoptotic and necrotic deaths. In contrast, when cells were exposed in 5 mM PB (pH 7.4), most of them (~ 95%) were in the stage of necrotic death, as indicated by the overlapped image. A similar phenomenon was also observed in the presence of BFP-AuNP sensors. When cells die due to necrosis, it results in the loss of cell membrane integrity and uncontrollable release of intracellular contents. It means that in the process of testing EDCs, GFP-AuNP sensors are capable of interacting with both cell membrane debris and intracellular network.

Furthermore, the cell stages at different doses were analyzed by flow cytometry. Measurements were performed with E2 or E2 + ICI treated BT549, MCF7 and T47D cells after 24 hour exposure. Before analysis by the flow cytometer, cells were treated with 70% ethanol at  $-20^{\circ}\text{C}$  and stained with PI. DNA contents and cell cycle distributions were analyzed using the Dean-Jett-Fox algorithm in FlowJo software (Figure 2.10). In all cases, the DNA content frequency histograms displayed low RMS (root mean square) scores and narrow  $G_1$  peaks with low coefficient of variance (CV). The E2 dose response curves using GFP-AuNP sensors were consistent to the changes in the cell cycle distribution (Figure 2.11a). For MCF7 cell line, the percentage of cells in S-phase increased with the concentrations of E2. In contrast, for T47D cell line, the increasing percentage of cells in  $G_0/G_1$ -phase and  $G_2/M$ -phase represents the growth of the cell number and protein

synthesis demonstrating strong responses by GFP-AuNP sensors. BT549 cell line did not display any significant changes in cell cycle, and the variations were less than 3% in total population. Interestingly, changes in G<sub>2</sub>/M-phase could be correlated to the cell lysate studies using GFP-AuNP sensors as well (Figure 2.11b).

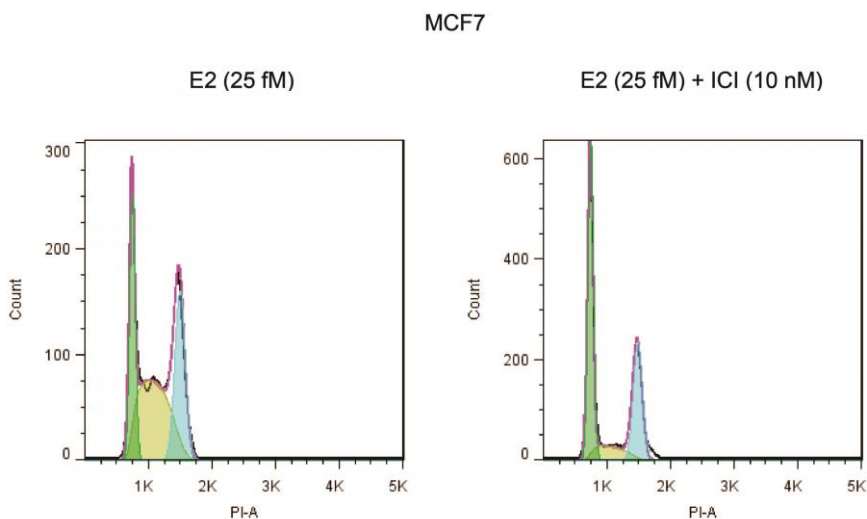


**Figure 2.10** Representative examples of DNA histograms obtained from BD LSR II. Green, yellow and cyan areas of histograms represent G<sub>1</sub>, S and G<sub>2</sub>/M phases.

Overall, our cell-based GFP-AuNP sensing method utilizes the necrotic cell death to detect stages of DNA synthesis, the cell number, changes on the cell plasma membrane, and protein expression levels. The responses of sensors indicate the quantitation of analytes.

### 2.3 Conclusions

This study demonstrates that the cell-based GFP-AuNP sensing method is a promising HTS tool to rapidly detect EDCs at ultra-low doses. It offers an easy and sensitive measurement of changes in stages of specific cells at a range of exposure concentrations and time. Forcing cell death in necrosis helps GFP-AuNP sensors indicate the intracellular genomic signaling pathway. The abilities to detect low dose effects and

display NMDRCs are additional values of our sensing method as compared to other *in vitro* EDC screening assays.

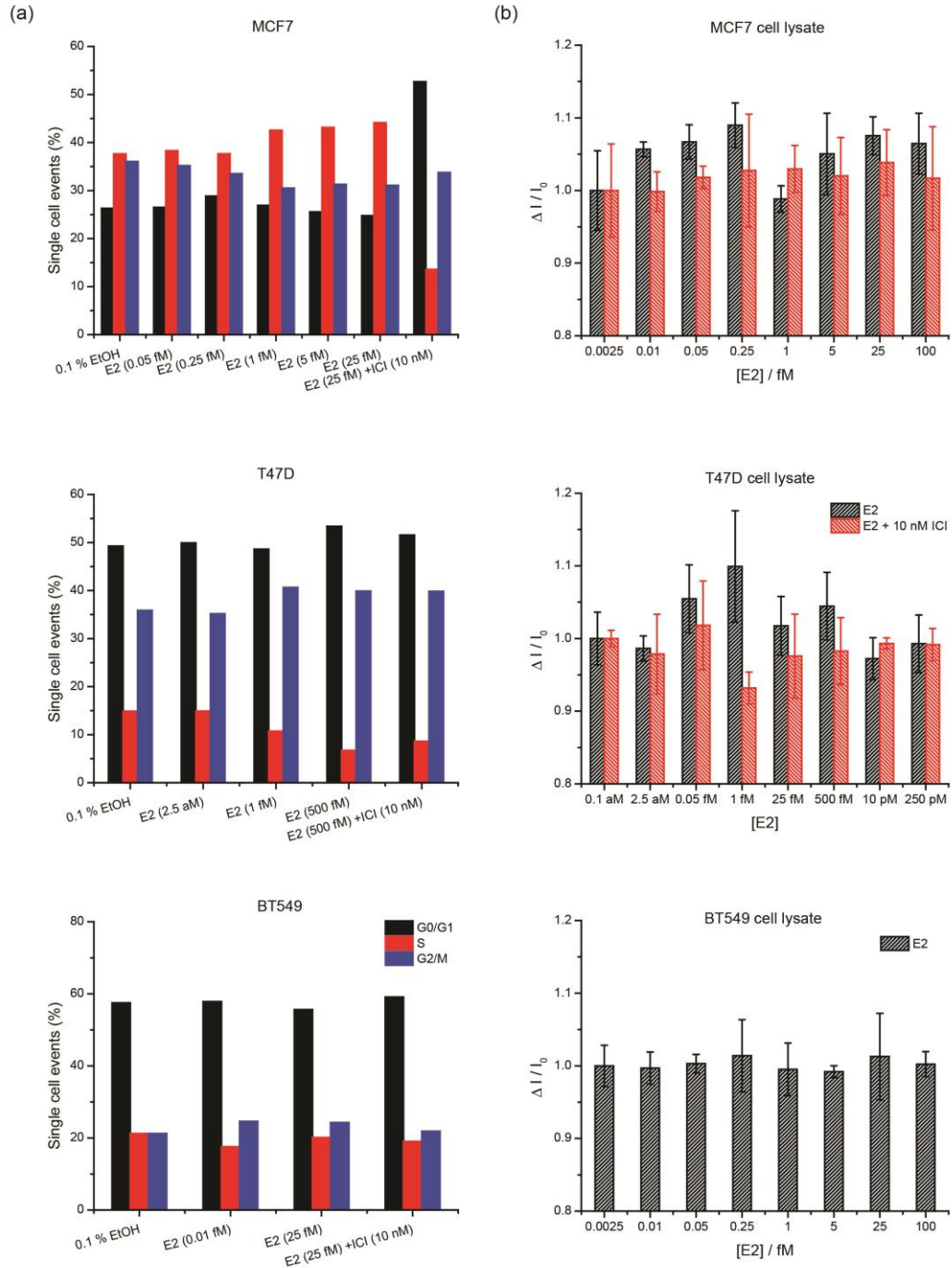


**Figure 2.11** (a) Comparison of cell cycle analysis on alcohol fixed cells after exposed to E2 and E2+ICI for 24 hours. 0.1% EtOH was used as control. (b) The dose-response relationships of cell lysates using GFP-AuNP sensors. The lysates were collected after the cells exposed to E2 and E2 + ICI for 24 hours.

## **2.4 Experimental Methods**

### **2.4.1 Comparison of measuring cell proliferation by GFP-AuNP complexes, alamar blue reagent and Hoechst 33342 stain**

A range of MCF7 cells (2,000-9,000 cells per well) were seeded in 96-well black-wall, clear bottom microplates with phenol red free DMEM/F-12 containing 2.5% DCC-FBS for overnight. The cells were washed by PBS twice before applying GFP-AuNP complexes, alamar blue reagent ( $\lambda_x/\lambda_m$ : 535 nm/590 nm), or Hoechst 33342 stain ( $\lambda_x/\lambda_m$ : 355 nm/460 nm). 100 nM cationic benzyl headgroup AuNP and 150 nM EGFP were mixed in 5 mM PB (pH 7.4) to form GFP-AuNP sensors. 10% alamar blue in serum-containing media was added for 3 hour 37<sup>0</sup>C incubation before measurements. Cells were incubated with Hoechst 33342 stain for 15 minutes and washed twice by PBS. The fluorescent intensities were monitored using Molecular Devices SpectraMax M3 microplate reader (at 25<sup>0</sup>C).

### **2.4.2 Cell-based sensing E2 and BPA using GFP-AuNP complexes and Hoechst 33342 stain**

MCF7, T47D, BT549 cell lines were initially cultured in DMEM containing 10% dialyzed FBS, 1% antibiotics (100 U/ml penicillin and 100  $\mu$ g/ml streptomycin). Cells were grown in a humidified 37<sup>0</sup>C incubator under a 5% CO<sub>2</sub> atmosphere. To maintain the consistent results, cells were split with a maximum of 20 passages. In all experiments, assays were performed under low steroid conditions with DCC-FBS. To minimize the estrogenic activity of serum and synchronize the cells in G<sub>0</sub>/G<sub>1</sub> phase of the cell cycle, phenol red-free DMEM/F-12 containing 5% DCC-FBS and 1% antibiotics was used to

treat the cells for 72 hours. Then, 125 uL 5000 cells per well were seeded in 96-well black-wall, clear-bottom microplates with phenol red free DMEM/F-12 containing 2.5% DCC-FBS and 1% antibiotics for another 24 hours before adding E2 or BPA. E2, BPA and ICI was dissolved in pure ethanol, protected from the light and stored at  $-20^{\circ}\text{C}$ . Final ethanol concentration in media did not exceed 0.2%. The plates were carefully washed by PBS buffer twice before applying GFP-AuNP sensors or Hoechst 33342 stain. The fluorescent intensities were measured on the microplate reader. The dose responses curves were fitted using the Hill equation.

### **2.4.3 Fluorescent imaging using YO-PRO-1 and PI stain**

5,000 MCF7 cells per well were placed in the 96-well clear bottom plates. YO-PRO-1 and PI stain were mixed in the respective media. The media was added to the cells after cells were washed twice in PBS buffer. After 30 minute incubation, the images were taken under the fluorescence microscope with blue and green excitation fluorescence filters. Instead of GFP-AuNP complexes, EBFP2 were applied to mix with the same AuNPs to avoid the green fluorescence interference with YO-PRO-1.

### **2.4.4 Flow cytometric analysis of MCF7, T47D and BT549 cells at different E2 doses**

60,000 MCF7, T47D and BT549 cells were seeded per well in 24-well plates and allowed to grow overnight. Cells were exposed to the same amount of E2 as previous studies for 24 hours. After trypsinized and centrifuged, cells were added 70% ethanol and incubated at  $-20^{\circ}\text{C}$  for 2 hours minimum. Then ethanol was removed and PI/RNase stain was added. After 15 minute incubation, data of 10,000 single cell events were collected

with BD LSR II flow cytometer using a 488 nm excitation laser and a 575/26 nm bandpass filter. With cell doublets and aggregates gated out, the DNA content histograms were analyzed using FlowJo software.

#### **2.4.5 Cell lysate studies using GFP-AuNP complexes**

Cells were seeded in 24-well plates as the previous study. After 24 hour E2 exposure, cells were washed by PBS twice and treated by lysis buffer [0.15 mmol/L NaCl, 5 mmol/L EDTA, 1% Triton-X 100, 10 mmol/L Tris-HCl (pH 7.4), plus half of a tablet of complete protease inhibitor cocktail in 50 mL buffer] for 10 minutes at 4<sup>0</sup>C. The lysates were spun down at 4<sup>0</sup>C for 15 min at 14000 rpm and ~200 ng of the supernatants were analyzed by GFP-AuNP sensors.

#### **2.5 References**

1. Gibson, C. L. *Perspectives in Biology and Medicine* **2010**, *53*, 152–155.
2. Marino, M.; Galluzzo, P.; Ascenzi, P. *Current genomics* **2006**, *7*, 497.
3. Nelson, L. R.; Bulun, S. E. *J. Am. Acad. Dermatol.* **2001**, *45*, S116–124.
4. Gronemeyer, H.; Gustafsson, J.-Å.; Laudet, V. *Nat Rev Drug Discov* **2004**, *3*, 950–964.
5. Prossnitz, E. R.; Barton, M. *Nat Rev Endocrinol* **2011**, *7*, 715–726.
6. Diamanti-Kandarakis, E.; Bourguignon, J.-P.; Giudice, L. C.; Hauser, R.; Prins, G. S.; Soto, A. M.; Zoeller, R. T.; Gore, A. C. *Endocrine Reviews* **2009**, *30*, 293–342.
7. Diduch, M.; Polkowska, Ż.; Namieśnik, J. *J Expos Sci Environ Epidemiol* **2013**, *23*, 111–119.
8. Vandenberg, L. N.; Colborn, T.; Hayes, T. B.; Heindel, J. J.; Jacobs, D. R.; Lee, D.-H.; Shioda, T.; Soto, A. M.; vom Saal, F. S.; Welshons, W. V.; Zoeller, R. T.; Myers, J. P. *Endocrine Reviews* **2012**, *33*, 378–455.

9. Kumar, R.; Zakharov, M. N.; Khan, S. H.; Miki, R.; Jang, H.; Toraldo, G.; Singh, R.; Bhasin, S.; Jasuja, R. *Journal of Amino Acids* **2011**, 2011.
10. Norman, A. W.; Mizwicki, M. T.; Norman, D. P. G. *Nat Rev Drug Discov* **2004**, 3, 27–41.
11. Melnick, R.; Lucier, G.; Wolfe, M.; Hall, R.; Stancel, G.; Prins, G.; Gallo, M.; Reuhl, K.; Ho, S.-M.; Brown, T.; Moore, J.; Leakey, J.; Haseman, J.; Kohn, M. *Environ Health Perspect* **2002**, 110, 427–431.
12. Vandenberg, L. N.; Ehrlich, S.; Belcher, S. M.; Ben-Jonathan, N.; Dolinoy, D. C.; Hugo, E. R.; Hunt, P. A.; Newbold, R. R.; Rubin, B. S.; Saili, K. S.; Soto, A. M.; Wang, H.-S.; Saal, F. S. vom. *Endocrine Disruptors* **2013**, 1, 0–1.
13. Calabrese, E. J.; Baldwin, L. A. *Hum Exp Toxicol* **2002**, 21, 91–97.
14. Reddel, R. R.; Sutherland, R. L. *Eur J Cancer Clin Oncol* **1984**, 20, 1419–1424.
15. Calabrese, E. J. *Br J Clin Pharmacol* **2008**, 66, 594–617.
16. Zacharewski, T. *Environmental science & technology* **1997**, 31, 613–623.
17. Yang, C. Z.; Yaniger, S. I.; Jordan, V. C.; Klein, D. J.; Bittner, G. D. *Environmental health perspectives* **2011**, 119, 989.
18. Vanparys, C.; Maras, M.; Lenjou, M.; Robbens, J.; Van Bockstaele, D.; Blust, R.; De Coen, W. *Toxicology in Vitro* **2006**, 20, 1238–1248.
19. Cavailles, V.; Garcia, M.; Rochefort, H. *Mol. Endocrinol.* **1989**, 3, 552–558.
20. Bondy, K. L.; Zacharewski, T. R. *Nucleic Acids Res* **1993**, 21, 5277–5278.
21. Poulin, R.; Baker, D.; Poirier, D.; Labrie, F. *Breast Cancer Res. Treat.* **1991**, 17, 197–210.
22. Gesztelyi, R.; Zsuga, J.; Kemeny-Beke, A.; Varga, B.; Juhasz, B.; Tosaki, A. *Arch. Hist. Exact Sci.* **2012**, 66, 427–438.
23. Henshel, D. S.; Black, M. C.; Harrass, M. C. *Environmental Toxicology and Risk Assessment: Standardization of Biomarkers for Endocrine Disruption and Environmental Assessment. Eighth volume*; ASTM International, 1999.
24. Bajaj, A.; Rana, S.; Miranda, O. R.; Yawe, J. C.; Jerry, D. J.; Bunz, U. H. F.; Rotello, V. M. *Chemical Science* **2010**, 1, 134.

## BIBLIOGRAPHY

- Anker, J. N.; Hall, W. P.; Lyandres, O.; Shah, N. C.; Zhao, J.; Van Duyne, R. P. *Nat Mater* 2008, 7, 442–453.
- Bajaj, A.; Miranda, O. R.; Phillips, R.; Kim, I.-B.; Jerry, D. J.; Bunz, U. H. F.; Rotello, V. M. *Journal of the American Chemical Society* 2010, 132, 1018–1022.
- Bajaj, A.; Rana, S.; Miranda, O. R.; Yawe, J. C.; Jerry, D. J.; Bunz, U. H. F.; Rotello, V. M. *Chemical Science* 2010, 1, 134.
- Bandyopadhyay, S.; Ni, J.; Ruggiero, A.; Walshe, K.; Rogers, M. S.; Chattopadhyay, N.; Glicksman, M. A.; Rogers, J. T. *J Biomol Screen* 2006, 11, 469–480.
- Bayraktar, H.; Ghosh, P. S.; Rotello, V. M.; Knapp, M. J. *Chem. Commun.* 2006, 1390–1392.
- Bondy, K. L.; Zacharewski, T. R. *Nucleic Acids Res* 1993, 21, 5277–5278.
- Bunz, U. H. F.; Rotello, V. M. *Angewandte Chemie International Edition* 2010, 49, 3268–3279.
- Calabrese, E. J. *Br J Clin Pharmacol* 2008, 66, 594–617.
- Calabrese, E. J.; Baldwin, L. A. *Hum Exp Toxicol* 2002, 21, 91–97.
- Carmody, L. C.; Germain, A. R.; VerPlank, L.; Nag, P. P.; Muñoz, B.; Perez, J. R.; Palmer, M. *J Biomol Screen* **2012**, 1087057112458317.
- Cavailles, V.; Garcia, M.; Rochefort, H. *Mol. Endocrinol.* 1989, 3, 552–558.
- Daniel, M.-C.; Astruc, D. *Chem. Rev.* 2004, 104, 293–346.
- De, M.; Rana, S.; Akpınar, H.; Miranda, O. R.; Arvizo, R. R.; Bunz, U. H. F.; Rotello, V. M. *Nature Chemistry* 2009, 1, 461–465.
- De, M.; You, C.-C.; Srivastava, S.; Rotello, V. M. *J. Am. Chem. Soc.* 2007, 129, 10747–10753.
- Diamanti-Kandarakis, E.; Bourguignon, J.-P.; Giudice, L. C.; Hauser, R.; Prins, G. S.; Soto, A. M.; Zoeller, R. T.; Gore, A. C. *Endocrine Reviews* 2009, 30, 293–342.
- Diduch, M.; Polkowska, Ž.; Namieśnik, J. *J Expos Sci Environ Epidemiol* 2013, 23, 111–119.
- Dix, D. J.; Houck, K. A.; Martin, M. T.; Richard, A. M.; Setzer, R. W.; Kavlock, R. J. *Toxicol. Sci.* 2007, 95, 5–12.

Eglen, R. M.; Bosse, R.; Reisine, T. *ASSAY and Drug Development Technologies* 2007, 5, 425–452.

Elci, S. G.; Moyano, D. F.; Rana, S.; Tonga, G. Y.; Phillips, R. L.; Bunz, U. H. F.; Rotello, V. M. *Chemical Science* 2013, 4, 2076.

Elghanian, R.; Storhoff, J. J.; Mucic, R. C.; Letsinger, R. L.; Mirkin, C. A. *Science* 1997, 277, 1078–1081.

Gesztelyi, R.; Zsuga, J.; Kemeny-Beke, A.; Varga, B.; Juhasz, B.; Tosaki, A. *Arch. Hist. Exact Sci.* 2012, 66, 427–438.

Gibson, C. L. *Perspectives in Biology and Medicine* 2010, 53, 152–155.

Gnanadesikan, R. *Discriminant Analysis and Clustering*; National Academies Press, 1988.

Greene, N. T.; Shimizu, K. D. *J. Am. Chem. Soc.* 2005, 127, 5695–5700.

Gronemeyer, H.; Gustafsson, J.-Å.; Laudet, V. *Nat Rev Drug Discov* 2004, 3, 950–964.

Henshel, D. S.; Black, M. C.; Harrass, M. C. *Environmental Toxicology and Risk Assessment: Standardization of Biomarkers for Endocrine Disruption and Environmental Assessment*. Eighth volume; ASTM International, 1999.

Huang, R.; Xia, M.; Cho, M.-H.; Sakamuru, S.; Shinn, P.; Houck, K. A.; Dix, D. J.; Judson, R. S.; Witt, K. L.; Kavlock, R. J.; Tice, R. R.; Austin, C. P. *Environ Health Perspect* 2011, 119, 1142–1148.

Inglese, J.; Johnson, R. L.; Simeonov, A.; Xia, M.; Zheng, W.; Austin, C. P.; Auld, D. S. *Nature Chemical Biology* 2007, 3, 466–479.

King, P. D.; Perry, M. C. *The Oncologist* 2001, 6, 162–176.

Klaassen, C. *Casarett & Doull's Toxicology: The Basic Science of Poisons, Eighth Edition (Casarett & Doull's Toxicology)*; 8 edition.; McGraw-Hill Professional, 2013.

Kumar, R.; Zakharov, M. N.; Khan, S. H.; Miki, R.; Jang, H.; Toraldo, G.; Singh, R.; Bhasin, S.; Jasuja, R. *Journal of Amino Acids* 2011, 2011.

Lowery, R. G.; Kleman-Leyer, K. *Expert Opinion on Therapeutic Targets* 2006, 10, 179–190.

Majumdar, S. K.; Valdellon, J. A.; Brown, K. A. *J Biomed Biotechnol* 2001, 1, 99–107.

Marino, M.; Galluzzo, P.; Ascenzi, P. *Current genomics* 2006, 7, 497.

Melnick, R.; Lucier, G.; Wolfe, M.; Hall, R.; Stancel, G.; Prins, G.; Gallo, M.; Reuhl, K.; Ho, S.-M.; Brown, T.; Moore, J.; Leakey, J.; Haseman, J.; Kohn, M. *Environ Health Perspect* 2002, 110, 427–431.

Nelson, L. R.; Bulun, S. E. *J. Am. Acad. Dermatol.* 2001, 45, S116–124.

Norman, A. W.; Mizwicki, M. T.; Norman, D. P. G. *Nat Rev Drug Discov* 2004, 3, 27–41.

Phillips, R. L.; Miranda, O. R.; You, C.-C.; Rotello, V. M.; Bunz, U. H. F. *Angewandte Chemie International Edition* 2008, 47, 2590–2594.

Poulin, R.; Baker, D.; Poirier, D.; Labrie, F. *Breast Cancer Res. Treat.* 1991, 17, 197–210.

Prossnitz, E. R.; Barton, M. *Nat Rev Endocrinol* 2011, 7, 715–726.

Rana, S. *Effective biosensor arrays using gold nanoparticle-protein conjugates*. Ph.D., University of Massachusetts Amherst: United States -- Massachusetts, 2013.

Rana, S.; Singla, A. K.; Bajaj, A.; Elci, S. G.; Miranda, O. R.; Mout, R.; Yan, B.; Jirik, F. R.; Rotello, V. M. *ACS Nano* 2012, 6, 8233–8240.

Reddel, R. R.; Sutherland, R. L. *Eur J Cancer Clin Oncol* 1984, 20, 1419–1424.

Reichling, L. J.; Lebakken, C. S.; Riddle, S. M.; Vedvik, K. L.; Robers, M. B.; Kopp, L. M.; Bruinsma, R.; Vogel, K. W. *J Biomol Screen* 2008, 13, 238–244.

Rosi, N. L.; Mirkin, C. A. *Chem. Rev.* 2005, 105, 1547–1562.

Saha, K.; Agasti, S. S.; Kim, C.; Li, X.; Rotello, V. M. *Chemical Reviews* 2012, 112, 2739–2779.

Schoonen, W. G. E. J.; Westerink, W. M. A.; Horbach, G. J. In *Molecular, Clinical and Environmental Toxicology*; Luch, A., Ed.; *Experientia Supplementum*; Birkhäuser Basel, 2009; pp. 401–452.

Sheehan, P. E.; Whitman, L. J. *Nano Lett.* 2005, 5, 803–807.

Shipway, A. N.; Katz, E.; Willner, I. *ChemPhysChem* 2000, 1, 18–52.

Stoeva, S. I.; Lee, J.-S.; Thaxton, C. S.; Mirkin, C. A. *Angewandte Chemie International Edition* 2006, 45, 3303–3306.

Su, K.-H.; Wei, Q.-H.; Zhang, X.; Mock, J. J.; Smith, D. R.; Schultz, S. *Nano Lett.* 2003, 3, 1087–1090.

Vandenberg, L. N.; Colborn, T.; Hayes, T. B.; Heindel, J. J.; Jacobs, D. R.; Lee, D.-H.; Shioda, T.; Soto, A. M.; vom Saal, F. S.; Welshons, W. V.; Zoeller, R. T.; Myers, J. P. *Endocrine Reviews* 2012, 33, 378–455.

Vandenberg, L. N.; Ehrlich, S.; Belcher, S. M.; Ben-Jonathan, N.; Dolinoy, D. C.; Hugo, E. R.; Hunt, P. A.; Newbold, R. R.; Rubin, B. S.; Sali, K. S.; Soto, A. M.; Wang, H.-S.; Saal, F. S. *Endocrine Disruptors* 2013, 1, 0–1.

Vanparys, C.; Maras, M.; Lenjou, M.; Robbens, J.; Van Bockstaele, D.; Blust, R.; De Coen, W. *Toxicology in Vitro* 2006, 20, 1238–1248.

Xia, M.; Huang, R.; Witt, K. L.; Southall, N.; Fostel, J.; Cho, M.-H.; Jadhav, A.; Smith, C. S.; Inglese, J.; Portier, C. J.; Tice, R. R.; Austin, C. P. *Environ Health Perspect* 2008, 116, 284–291.

Yang, C. Z.; Yaniger, S. I.; Jordan, V. C.; Klein, D. J.; Bittner, G. D. *Environmental health perspectives* 2011, 119, 989.

You, C.-C.; De, M.; Rotello, V. M. *Org. Lett.* 2005, 7, 5685–5688.

You, C.-C.; Miranda, O. R.; Gider, B.; Ghosh, P. S.; Kim, I.-B.; Erdogan, B.; Krovi, S. A.; Bunz, U. H. F.; Rotello, V. M. *Nature Nanotechnology* 2007, 2, 318–323.

Zacharewski, T. *Environmental science & technology* 1997, 31, 613–623.

Zhang, R.; Beyer, B. M.; Durkin, J.; Ingram, R.; Njoroge, F. G.; Windsor, W. T.; Malcolm, B. A. *Analytical Biochemistry* 1999, 270, 268–275.

Zheng, W.; Spencer, R. H.; Kiss, L. *ASSAY and Drug Development Technologies* 2004, 2, 543–552.